



Microstructural characterization of atomized U 3 Si 2 powders with different silicon contents (7.4-7.8 wt%)

X. Iltis, J. Havette, V. Klosek, C. Onofri, K.H. Lee, J.H. Kim, Y.J. Jeong, M. Pasturel, H. Palancher

► To cite this version:

X. Iltis, J. Havette, V. Klosek, C. Onofri, K.H. Lee, et al.. Microstructural characterization of atomized U 3 Si 2 powders with different silicon contents (7.4-7.8 wt%). Journal of Nuclear Materials, 2023, 573, pp.154141. 10.1016/j.jnucmat.2022.154141 . hal-03956503

HAL Id: hal-03956503

<https://univ-rennes.hal.science/hal-03956503>

Submitted on 25 Jan 2023

HAL is a multi-disciplinary open access archive for the deposit and dissemination of scientific research documents, whether they are published or not. The documents may come from teaching and research institutions in France or abroad, or from public or private research centers.

L'archive ouverte pluridisciplinaire **HAL**, est destinée au dépôt et à la diffusion de documents scientifiques de niveau recherche, publiés ou non, émanant des établissements d'enseignement et de recherche français ou étrangers, des laboratoires publics ou privés.



Distributed under a Creative Commons Attribution - NonCommercial 4.0 International License

Microstructural characterization of atomized U₃Si₂ powders with different silicon contents (7.4-7.8 wt%)

X. Iltis^{1*}, J. Havette^{1,3}, V. Klosek¹, C. Onofri¹, K.H. Lee², J.H. Kim², Y.J. Jeong², M. Pasturel³, H. Palancher¹

¹CEA, DES, IRESNE, DEC, Cadarache, F-13108 Saint-Paul-Lez-Durance, France

²Korea Atomic Energy Research Institute, 111 Daedeok-daero 989beon-gil, Yuseong-gu, Daejeon 34057, Republic of Korea

³Université de Rennes, CNRS, Institut des Sciences Chimiques de Rennes – UMR6226, F-35042 Rennes, France

*corresponding author: xaviere.iltis@cea.fr

ABSTRACT:

Atomization processes are used to produce uranium-based powders for the manufacturing of dispersion fuel for nuclear research reactors. Whereas this process is considered worldwide as a reference for U-Mo powder production, its use for U₃Si₂ is still limited.

In this paper, the microstructure of as-atomized nearly stoichiometric (7.4 wt% Si) and hyper-stoichiometric (7.6 and 7.8 wt% Si) U₃Si₂ powders is studied in detail. A wide range of analytical techniques were applied: X-ray diffraction (XRD), scanning electron microscopy (SEM) and scanning transmission electron microscopy (STEM), electron backscattered diffraction (EBSD) and energy dispersive X-ray spectroscopy (EDS) at both micrometer (SEM) and nanometer (STEM) scales. These analyses lead to an original description of the microstructure of these as-atomized U₃Si₂ particles.

It is shown that most of atomized particles contain only a few U₃Si₂ grains, some being even monocrystalline. The main secondary phase present in hyper-stoichiometric batches is an U₂₀Si₁₆C₃-like phase. Other minor phases are also encountered, some of them containing metallic impurity elements. These features are attributed to the uranium raw material composition and to a slight contamination by carbon during the powder synthesis.

The nature and morphology of secondary phases present in U₃Si₂ atomized particles appear thus to be linked not only to the silicon excess but also to the presence of impurities which probably strongly segregate during the very fast solidification of the alloy droplets. A slight superficial oxidation of particles also occurs and induces a local redistribution of silicon.

Keywords: U₃Si₂, atomization, microstructure, impurities, segregation.

1. INTRODUCTION

Material Testing Reactors (MTRs) are used primarily to study materials under irradiation and to produce radioisotopes for medical and industrial applications. The fuel elements of MTRs are most often made of plates in which the fissile material in powder form is dispersed within an aluminium matrix, to form a fuel core cladded between two aluminium alloy sheets [1].

In the 1980's due to nuclear proliferation issues related to high enriched uranium ($>20\% \text{ }^{235}\text{U}$) it was decided to convert research reactors to low enriched uranium fuel ($<20\% \text{ }^{235}\text{U}$) [2]. To balance the reduced enrichment new nuclear fuels with higher densities were developed to replace the previous ones (which were mainly UAl_x and U_3O_8) [3].

The main candidates are now U-Mo (a uranium-molybdenum alloy with a Mo content typically comprised between 7 and 10 wt%) and U_3Si_2 (a line compound with a Si amount of 7.3 wt%). For U-Mo powder manufacturing, centrifugal atomization is the reference process [4] [5].

U_3Si_2 powders are produced so far by arc-melting followed by comminution [6]. Indeed, grinding this brittle compound is the reference process on both laboratory [7] [8] and industrial scales [9]. U_3Si_2 particles are then mixed with aluminium powder and pressed to form the fuel core which is cladded by aluminium alloy sheets. The plate is then hot and cold rolled. This process commonly named "picture-frame technique" is the reference one and has been applied for years [9]. However, some limitations are encountered with this manufacturing method especially for high loaded fuel plates required by high performance MTRs. First, it is not possible to control particles morphology and size (except by sieving) [8]. Second, with such a powder, large particles with sharp edges can sometimes penetrate the cladding locally and reduce its thickness [1]. Third, during the plate fabrication by rolling, particles are fragmented, inducing porosities which are difficult to control [1]. Particles can also align along the rolling direction, potentially leading to anisotropic thermal properties [10]. Fourth, the angular shape of those particles induces powder flowability characteristics which are not well-adapted for rolling [11].

The above cited limitations can be overcome or at least their consequence can be reduced by using spherical U_3Si_2 particles. That is why the Korea Atomic Energy Research Institute (KAERI) has developed centrifugal atomization applied to U_3Si_2 . The first mention of the implementation of this process to produce U_3Si_2 in the open literature dates from 1997 [11] [12]. It consists in pouring a molten liquid of a composition $3\text{U}+2\text{Si}$ onto a rotating disk. Under the effect of centrifugal force, droplets are ejected in the inert chamber of the atomizer and solidify in spherical shape.

This process allows the formation of spherical particles with narrow size distribution that can be controlled by modifying the pouring rate or the disk rotation speed [12]. Furthermore, spherical particles have 30% less specific surface area than comminuted ones, resulting in a smaller interface with Al [13]. This characteristic can be valuable to limit the interaction between U_3Si_2 particles and Al matrix in fuel plates which occurs during in-pile irradiation, as this reaction consumes the Al matrix which exhibits a high thermal conductivity. This point was checked using out-of-pile annealing experiments: $\text{U}_3\text{Si}_2/\text{Al}$ dispersions made of comminuted or atomized particles were thermally annealed and a smaller volume increase was obtained for the dispersion made of atomized particles [13]. However, the atomized particles confer a lower mechanical resistance to the green compact, the main contribution to the latter coming from the contacts between the U_3Si_2 particles and the Al particles constituting the matrix [4]. Finally, atomized particles induce less as-fabricated porosity in the fuel meat than comminuted ones for a given volume fraction of U_3Si_2 which can be valuable for nuclear fuel developers.

The advantages that atomized particles could bring to the high-performance research reactors conversion initiative are therefore very significant. They led to the design and fabrication of a fuel element made of plates containing U_3Si_2 atomized powders in the frame of an irradiation test named KIMQI (for KAERI high density atoMized silicide fuel Qualification Irradiation) launched in 2021 in Belgium Reactor 2 (BR2) [14].

Regarding microstructural features, the first analyses of U_3Si_2 atomized particles mentioned small U_3Si_2 grains with Si-rich phases at grain boundaries identified as USi and USi_2 [11] [12]. More recently, Yang *et al.* studied the oxidation behaviour of U_3Si_2 atomized powders [15]. The brief analysis of the fresh powders reported in their publication pointed out the presence of UO_2 on the surface of the particles and Si segregation at grain boundaries in their core. They also mentioned dendrite-like grains and finally concluded that a more detailed work was needed to understand the solidification mechanisms and resulting compositional segregation phenomena in the U_3Si_2 system.

The present paper aims at supplementing the existing available microstructural characterizations of these fresh powders. Electron backscattered diffraction (EBSD) was recently successfully applied to arc-melted U_3Si_2 and brought new insights in its characterization [8]. It appears thus interesting to use this method for studying atomized particles and to combine it with transmission electron microscopy. Furthermore, in accordance with the international recommendations for U_3Si_2 synthesis for its use as fuel for research reactors [16], slight Si hyper-stoichiometries were tested by KAERI [17]. In a previous work, the impact of a deviation from U_3Si_2 stoichiometry on the microstructure of arc-melted U_3Si_2 was studied and various secondary phases were observed depending on synthesis conditions [8]. In the same way, the present work seeks to obtain a wide overview of the structural and microstructural features of U_3Si_2 atomized powders with three specified different Si contents: 7.4, 7.6 and 7.8 wt% (*i.e.*, 40.4, 41.1 and 41.8 at%). Dedicated attention is paid to the nature of the secondary phases which were analysed by EDS down to nanometer scale within the core of the particles and at their surface.

2. MATERIALS AND METHODS

2.1 MATERIALS

U_3Si_2 powders used in this study were manufactured by KAERI using centrifugal atomization [12]. Three batches of U_3Si_2 powder were prepared with a depleted uranium and high purity silicon (99.999%) to have Si contents of 7.4, 7.6, and 7.8 wt%, respectively. For convenience, each batch is referred to as “batch A” (7.4 wt% Si), “batch B” (7.6 wt% Si), and “batch C” (7.8 wt% Si).

The chemical analysis results of each powder batch are gathered in Table 1. Si content is very close to the targeted value (even if it is a bit higher in the analysed sample from batch B: 7.7 instead of 7.6 wt%, that is 41.6 instead of 41.1 at%). Major impurities such as Al and Fe come from the depleted uranium, and the high carbon content of batch C is due to the erosion of carbon pouring rod during the atomization process. The oxygen content is almost the same ($\sim 1200 \mu\text{g.g}^{-1}$) in the three batches. It is also worth noting that the raw uranium batch used to synthesize these powders contains 0.21 wt% of vanadium. Regrettably, this element was not analysed in the atomized powders.

Whereas the U_3Si_2 powder atomization was run smoothly for batch A and C, some instabilities were noticed during the atomization of batch B; their occurrence should be kept in mind when interpreting the microstructure of U_3Si_2 particles from this powder batch.

Table 1: Chemical analysis of U₃Si₂ atomized powders (µg.g⁻¹ or *wt% (at%)).

Element	Batch A	Batch B	Batch C
*Si	7.41 (40.4)	7.73 (41.6)	7.81 (41.9)
C	418	150	1190
H	10	4	14
O	1263	1190	1160
N	10	25	10
Al	1000	700	900
Fe	1100	600	900
Ni	100	92.7	100
Cu	39	61	77
Zn	<5.0	21.9	<5.0
Cd	<5.0	<5.0	<5.0
Co	<5.0	<5.0	5.6
Li	<5.0	<5.0	<5.0
B	<5.0	<5.0	7.8

2.2 SAMPLE PREPARATION AND CHARACTERIZATION METHODS

Particles of each batch were dispersed on a conductive carbon tape, to be observed by scanning electron microscopy (SEM) in their as-received state. In order to be able to study their internal microstructure, some particles were mixed with aluminium powder and pressed to obtain a compact. This compact was mechanically polished, allowing to observe the particles in cross-section. A dedicated gentle polishing method with a colloidal silica solution was used before analyses by EBSD [8] [18]. For X-ray diffraction (XRD) measurements, particles were dispersed in an oxygen-free solvent (cyclohexane) and manually crushed in a mortar under air in order to obtain representative information about the phases present at their periphery and in their core. This mixture was then put onto a single crystalline silicon holder and analyses were performed after the evaporation of the solvent.

Granulometric distribution and morphological characteristics of atomized powders were determined by image analysis, using the ImageJ freeware. Analyses were based on SEM images of particles dispersed on a carbon tape. About 2000 particles per batch were considered. Images were binarized and automatically analysed to acquire quantitative information. For granulometric distribution, the area of each particle was detected and converted to an equivalent circular diameter (ECD). Regarding shape analysis, the roundness parameter was calculated as:

$$\text{Roundness} = 4A / \pi * \text{MFD}^2 (1)$$

with A, the area of the particle and MFD, the maximum Feret diameter, defined as the distance between two parallel tangents to the particle delimitating its maximum diameter. With this parameter, a perfectly spherical particle has a roundness of 1, while an angular particle has a roundness of 0.3 to 0.5.

XRD measurements were performed with a Bragg-Brentano θ-θ Bruker D8 Advance X-ray diffractometer using copper radiation from a conventional tube source (Kα1+ Kα2 radiation: λ=1.5406 and 1.5444 Å). The angular range analysed was 10-140° with a 0.01° step and a counting time of 3 seconds per point. The samples rotated during their analysis. Diffraction data were refined with the Rietveld method, using the FullProf software [19]. A systematic refinement method was applied, using a sequential mode.

SEM examinations and analyses by energy dispersive spectrometry (EDS) were performed using a Nova NanoSEM 450 from FEI equipped with an Oxford Instruments EDS silicon drift detector with an

active surface of 80 mm². Working distance was set to 7 mm and high voltage to 15 kV. EDS data were processed with the AZTEC software, using its standard database for quantification of elements.

Lamellas were prepared from atomized particles by focused ion beam (FIB) milling with a dual beam SEM-FIB from FEI (Helios 600 NanoLab) using a classical lift-out method [20]. These lamellas were observed with a ThermoFisher Scientific Talos F200X transmission electron microscope (TEM) equipped with four ThermoFisher Scientific in-column EDS detectors. This microscope was mainly operated in scanning mode (STEM), using a high angle annular dark field (HAADF) detector. EDS data were processed with the VELOX software, using its standard data base without sample absorption corrections. These nano-EDS data collected with a spatial resolution of a few nanometers should nicely supplement EDS analyses performed at SEM scale *i.e.*, with a spatial resolution at best around a few tenths of a micrometer. Electron diffraction patterns were also acquired on selected areas. They were indexed with the CrystTBx software [21].

EBSL analyses were achieved with the Nova NanoSEM 450. This microscope is equipped with a Symmetry camera (maximum resolution: 1244x1024 pixels) from Oxford Instruments. AZTEC and AZTEC Crystal softwares were respectively used for data collection and analysis. Acquisitions were made with a 70° tilt, a 15 mm working distance, a high voltage of 20 kV and a beam current of about 10 nA. No camera binning was applied and the step size was adapted on a case-by-case basis. It was often of the order of 100 nanometers (that is not very far from the spatial resolution of EBSD, in standard conditions [22]).

The crystallographic structures used for refinement of XRD data and for indexation of EBSD maps and electron diffraction patterns are listed in Table 2. Several other binary and ternary silicides were also considered when treating these diffraction data. They are not listed in this table, as they did not turn out to be relevant.

Table 2: Phases, with their crystallographic characteristics, used for analysis of XRD, EBSD and electron diffraction patterns acquired on U₃Si₂ powders prepared by centrifugal atomization.

Phase	[Si]/([U]+[Si]) ratio + corresponding Si content*	Cell	Space group	a (Å)	b (Å)	c (Å)	Density (g/cm ³)	Reference
U ₃ Si ₂	2/5 – 40 at%	Tetragonal	P4/mmb (127)	7.330	-	3.900	12.2	[23]
U ₂₀ Si ₁₆ C ₃	4/9 – 44.4 at%	Hexagonal	P6/mmm (191)	10.38	-	8.01	11.7	[24]

(*) Si concentration (in at%) is calculated considering only U and Si.

3. RESULTS

3.1 GRANULOMETRIC DISTRIBUTION AND MORPHOLOGICAL CHARACTERISTICS OF THE PARTICLES

Figure 1 summarizes the results obtained by analysis of SEM images collected on about 2000 particles per batch, in terms of size (given by their equivalent circular diameter) and shape (given by their roundness). Particles were sieved at KAERI to eliminate those with diameters higher than 150 µm and few of them reach ECD values higher than 100 µm. For batches A and C, a monomodal size distribution in frequency is obtained with mean ECD values of 55 µm and 75 µm respectively. In the case of batch B, a more spread size distribution is observed (from 10 to 130 µm). This batch also exhibits less spherical particles. Indeed, only about 50% of them are characterized by a roundness of 1 (*i.e.*, are perfectly spherical) instead of more than 70% for batches A and C. These particularities are very likely linked to the instabilities noticed during the atomization step for batch B.

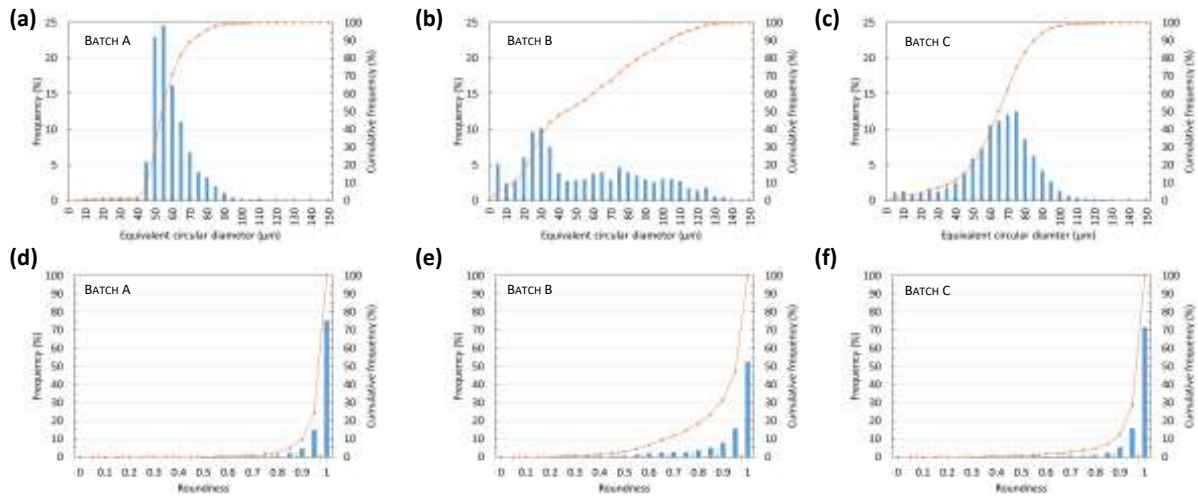


Figure 1: Morphological characteristics of U_3Si_2 powders prepared by centrifugal atomization as obtained by image analysis of SEM images: (a) (b) (c) size distribution in frequency (in blue) and cumulative frequency (in orange), and (d) (e) (f) roundness distribution in frequency (in blue) and cumulative frequency (in orange) obtained on particles from batches A, B and C, respectively.

3.2 XRD ANALYSES

Figure 2 gathers the three X-ray diffractograms (in the 10° - 60° 2θ range) acquired on crushed particles from each batch. As expected, U_3Si_2 is the majority phase. However, even in the case of batch A, with a nearly stoichiometric Si/U ratio, some low intensity peaks remain unindexed (see for example the two ones circled by a dotted black line). These little peaks are also present on the two other diffractograms, which tends to indicate that they should correspond to impurities present in the three batches. A set of additional peaks with intensity growing with silicon content is detected in batches B and C and is compatible with an $\text{U}_{20}\text{Si}_{16}\text{C}_3$ compound (considering the PDF® file n°654854, from the International Center for Diffraction Data). This phase, stabilized by carbon [25], is richer in silicon than U_3Si_2 , which is consistent with the silicon hyper-stoichiometry of these two last batches. It is worth noting that $\text{U}_{20}\text{Si}_{16}\text{C}_3$ has the same crystallographic structure as U_5Si_4 [26], and the same Si/U ratio, but with carbon atoms inserted in octahedral sites. It may correspond to a stabilized form of U_5Si_4 which is reported to be thermodynamically unstable [27] [28]. Altogether, the refinement of XRD data by the Rietveld method was slightly better when considering the $\text{U}_{20}\text{Si}_{16}\text{C}_3$ cell rather than U_5Si_4 . In fact, it would be more accurate to speak about a $\text{U}_{20}\text{Si}_{16}\text{C}_3$ -like phase, as its carbon content is not known and could be lower than 3/39 (7.7 at%).

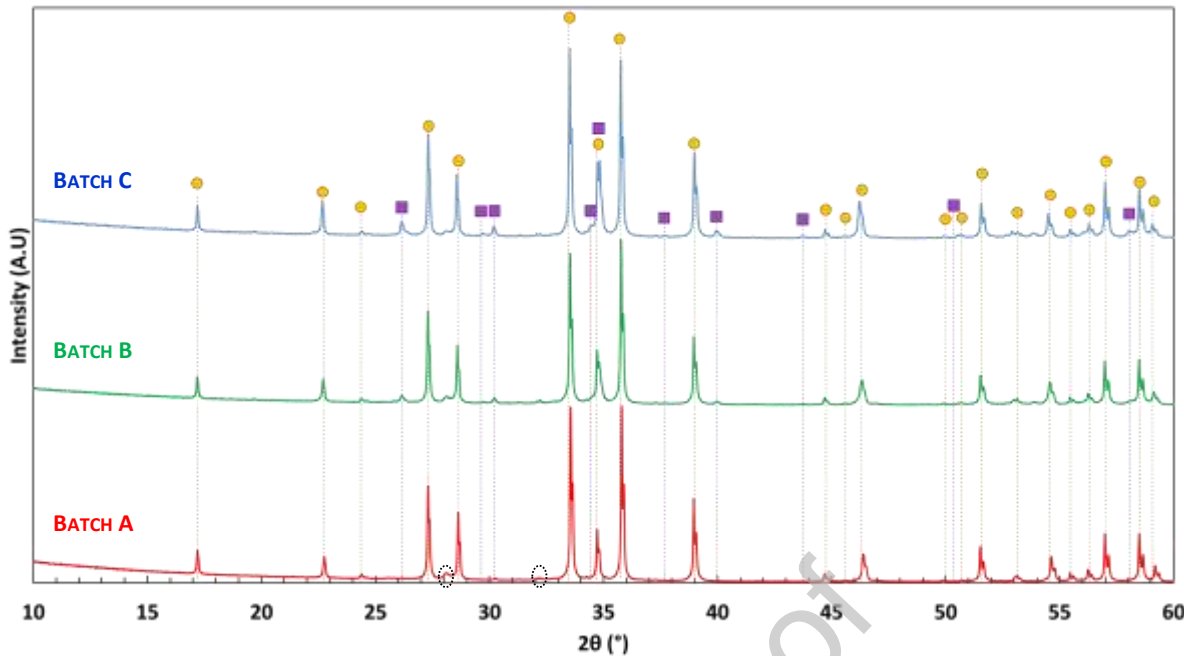


Figure 2: XRD patterns acquired on crushed powders from three batches of U_3Si_2 prepared by centrifugal atomization, indexed with U_3Si_2 (orange disks) and $\text{U}_{20}\text{Si}_{16}\text{C}_3$ -like (purple squares) phases.

Discrepancies between the measured and calculated relative intensities of the U_3Si_2 diffraction peaks were found with the three diffractograms, as illustrated in Figure 3 for batch C. Such differences, not attributable to preferential orientation effects, were also reported by other authors when studying U_3Si_2 powder batches obtained by comminuting arc-melted ingots [29] [30]. Their origin may be partly due to thermal displacement effects and/or to some structural disorder (i.e. fractional site occupation, point defects, etc.). Micro-absorption corrections following the procedure described in [31] for Bragg-Brentano diffraction geometry did not allow significantly improving the refinements, and appeared to strongly interfere with the quantitative analysis accuracy (as reported in [31]). Refinements were attempted, considering intrinsic defects such as those described by Middleburgh *et al.* [32] but instrumental resolution and diffraction data accuracy were too low for satisfactorily refining structural parameters such as occupation rates or displacement parameters. Despite these deviations, it was possible to estimate a weight fraction of $\text{U}_{20}\text{Si}_{16}\text{C}_3$ -like phase in the two Si hyper-stoichiometric batches, that is: 10(5) wt% for batch B and 21(5) wt% for batch C.

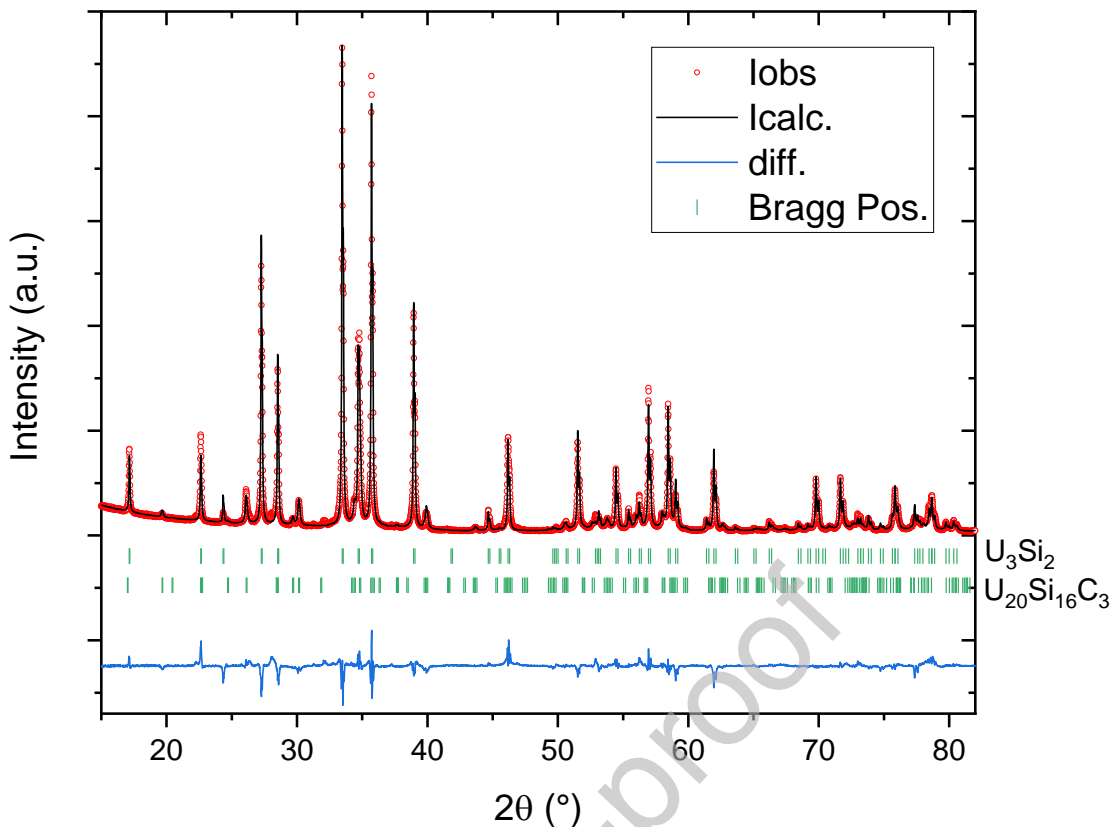


Figure 3: XRD pattern refined using the Rietveld method for batch C of atomized U_3Si_2 powder. The experimental data are plotted in red, the calculated ones in black and their difference is drawn in blue. The vertical green ticks indicate the Bragg peaks positions for U_3Si_2 and $\text{U}_{20}\text{Si}_{16}\text{C}_3$ -like phases. Agreement factors: $R_{\text{Bragg}}(\text{U}_3\text{Si}_2) = 9.8\%$; $R_{\text{Bragg}}(\text{U}_{20}\text{Si}_{16}\text{C}_3) = 19.6\%$; $\chi^2 = 24.0$.

3.3 EXAMINATIONS BY SEM AND EDS ANALYSES

3.3.1 Batch A (*almost stoichiometric in Si*)

Figure 4 summarizes the main features of U_3Si_2 particles from batch A, as evidenced by SEM imaging in backscattered electron mode (BSE). Figures 4a to 4c correspond to particles observed in their as received state, dispersed on a carbon tape. Their shape is nearly perfectly spherical, in accordance with the results of image analysis (Figure 1d). Their surface is characterized by the presence of geometrical networks with differences in grey levels, indicating the presence of different phases with different compositions. Submicron details with very fine lamellas (in light grey) can be observed at high magnification (Figure 4c). No superficial oxide layer seems to be present at this observation scale, even when observing fracture surfaces on broken particles at high magnification.

When the particles are observed in polished section (as in Figures 4d to 4f), darker phases than the U_3Si_2 matrix are evidenced. Note that the superficial layer which seems to be present all around the particle in Figure 4d corresponds actually to a border effect (a part of the particle located below the polished surface being visible). Dark phases form networks of fine veins which seem to be located at inter-dendritic spaces. Small voids probably due to local micro-shrinkage formed during the solidification of U_3Si_2 are also present in these areas. These veins could be made of different phases, as illustrated in Figure 4f where different grey levels can be seen within them.

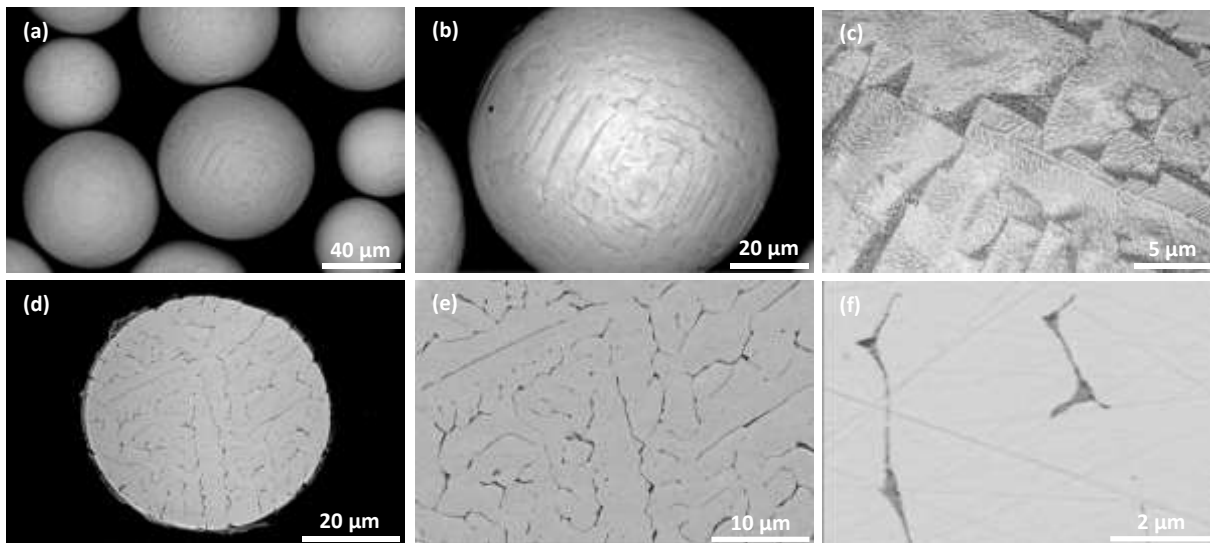


Figure 4: Electron micrographs obtained by SEM in BSE mode on particles from batch A of atomized U_3Si_2 powder: (a) (b) (c) as received state (three different magnifications), (d) (e) (f) after polishing (three different magnifications).

Numerous spot analyses were performed by EDS on such dark areas. As their lateral size does not exceed hundred nanometers, these analyses always include a contribution of the surrounding U_3Si_2 matrix (the resolution of EDS analyses being of the order of $1 \mu\text{m}^3$ on a massive sample). Figure 5a shows the location of different analysis points in a representative particle and Figure 5b summarizes the corresponding elemental composition results. Analyses performed in the matrix (positions 5 to 7) confirm that it corresponds to pure U_3Si_2 , with deviations lower than 1 at% from the theoretical composition values when excluding Al from the quantification. Indeed, it is believed that the 1 to 2 at% Al content measured by EDS in the U_3Si_2 matrix come from a surface contamination by the Al embedding medium.

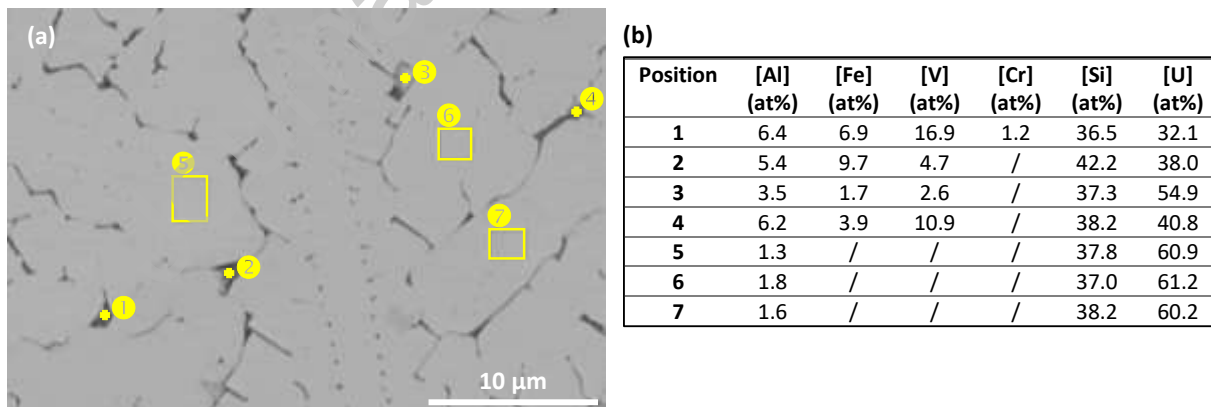


Figure 5: EDS analyses performed on a particle from batch A of atomized U_3Si_2 powder: (a) electron micrograph (SEM, BSE mode) showing the position of the analysed points in dark areas (points 1 to 4) and in the U_3Si_2 matrix (rectangles 5 to 7), (b) corresponding quantitative results.

Dark areas systematically contain metallic impurities, namely Al, Fe and V (and also some Cr in one case). Their Al content is presumably a bit overestimated as a result of the above-mentioned Al contamination of the particle surface. These secondary phases do not seem to contain a larger fraction of light impurities such as C or O than the matrix, knowing that C and O are present as contaminants on the whole sample surface and are thus difficult to quantify.

The relative content of metallic impurities varies from one area to another, which tends to indicate that they could correspond to a mixture of different phases.

On the basis of these results, it can be concluded that minor phases present in batch A probably correspond to a mixture of silicides containing uranium and metallic impurities. Their formation is very likely linked to segregation phenomena that occurred during U_3Si_2 solidification.

3.3.2 Batches B and C (hyper-stoichiometric in Si)

Figure 6 illustrates the characteristics of particles from batches B and C, in their as-received state and after polishing. Images from one or the other of these two batches are shown indifferently, as their features are similar.

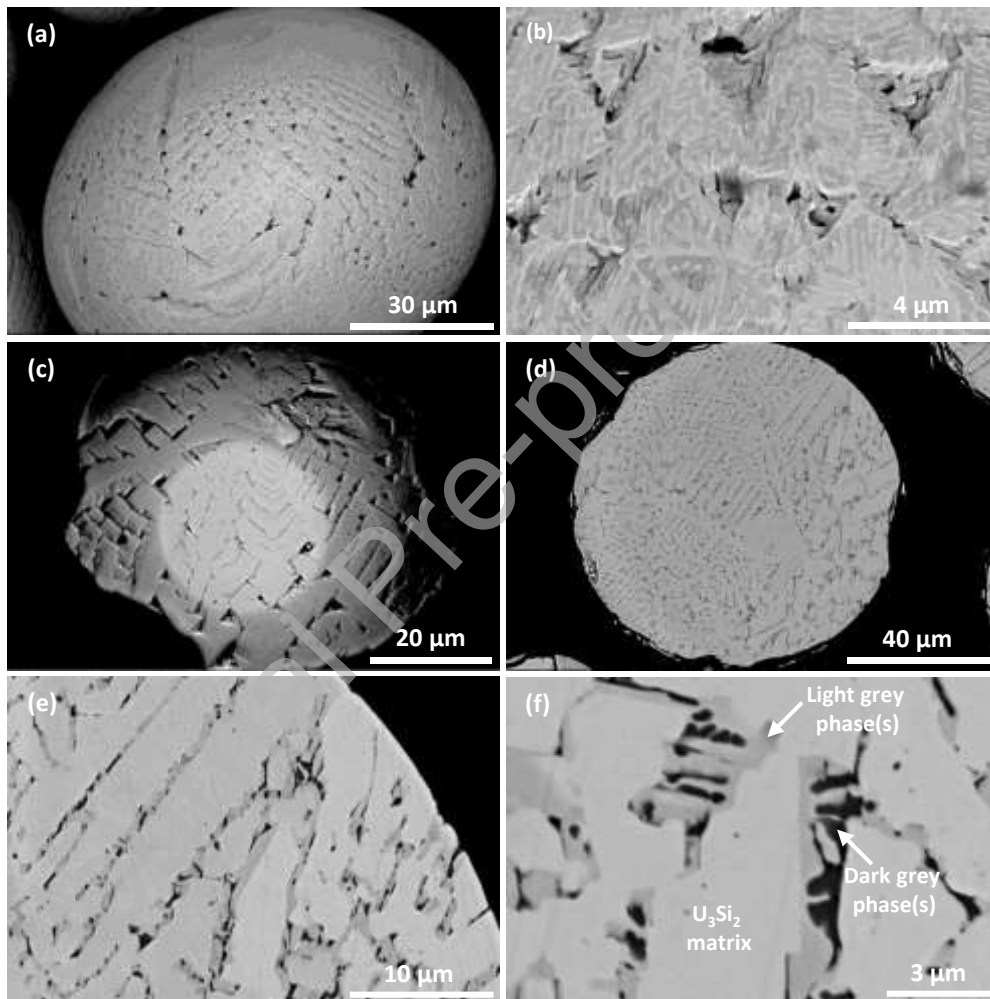


Figure 6: Electron micrographs obtained by SEM in BSE mode on particles from batches B and C of atomized U_3Si_2 powder: (a) (b) in the as-received state (two different magnifications, batch C), (c) after partial polishing (batch B), (d) (e) (f) after polishing (three different magnifications, batch C).

The geometrical networks already observed on the surface of particles from batch A are observed once again (Figures 6a and 6b) but the roughness associated with them seem to be higher. Very fine lamellas (in light grey) are visible again at high magnification (Figure 6b). A perfect continuity between the dark networks at the surface and those revealed in a polished section is noticed when observing partly polished particles (Figure 6c). Note that the non-spherical shape of the particle shown in Figure 6d is the consequence of mechanical polishing operations which induce a fragmentation of the periphery of some particles. As for batch A, polished sections reveal dark phases forming networks which seem to be located at inter-

dendritic spaces, but their veins are significantly thicker, especially in batch C. Observations performed at higher magnifications (Figures 6e and 6f) show that these veins contain different phases, according to the observed grey levels (see the annotations in Figure 6f).

EDS analyses were performed in many of these secondary phases. Typical results are presented in Figures 7 and 8, for light grey and dark grey phases respectively. They were achieved on batch C, where the veins are thicker and thus easier to characterize, but they are also representative of batch B.

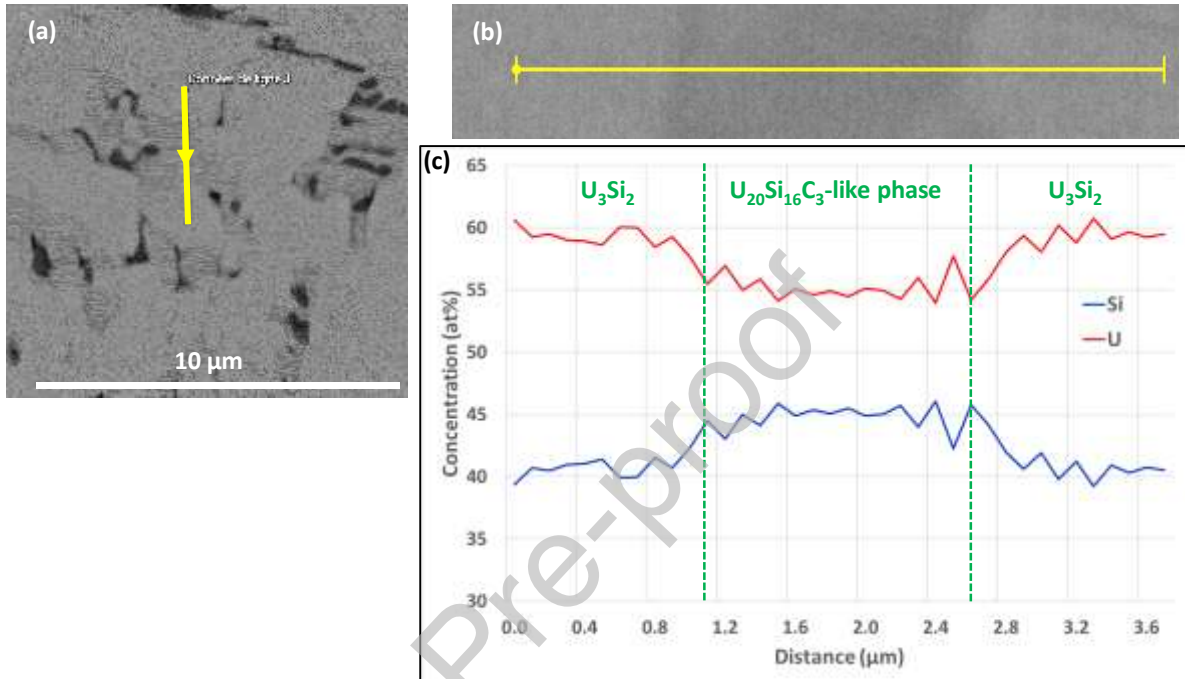


Figure 7: EDS analysis through a light grey secondary phase on a particle from batch C of atomized U_3Si_2 powder: (a) (b) electron micrographs (SEM, BSE mode) indicating the position of the line-scan (yellow lines), (c) corresponding composition profiles.

Light grey minor phases contain only two elements: Si and U (neglecting light elements such as C and O which are present on the whole surface of the sample as contaminants), as illustrated by Figure 7c, where green dotted lines delimitate a vein of such a phase. Note that their position does not exactly match that deduced from Figure 7b because of small drift that occurred during the analysis. Their Si amount is of the order of 45 at% and their $[\text{Si}]/([\text{U}]+[\text{Si}])$ ratio is close to 4/9. Such a ratio is that encountered in the U_5Si_4 and $\text{U}_{20}\text{Si}_{16}\text{C}_3$ -like phases. This result is consistent with the identification of an $\text{U}_{20}\text{Si}_{16}\text{C}_3$ -like phase by XRD, in batches B and C. No significant increase of the carbon content was noticed in that phase, probably due to the overall C-contamination of the sample surface.

Dark grey minor phases are most of the time characterized by a higher Si content than that of the U_3Si_2 matrix and also by the presence of metallic impurities such as V and Fe, that are heterogeneously distributed in their core, as shown by Figure 8c. In this example, the maximum Si content reaches about 55 at% but is very probably underestimated because of an averaging effect due to the surrounding matrix. Note that a slight increase in the Si composition profile (between 4-5 μm in Figure 8c) is associated to the crossing of a second vein of minor phases (probably thinner than the first one). The characteristics of these dark phases are similar to those of minor phases encountered in batch A (except the fact that Al is not present, in the analysed location), which tends to indicate that they are of the same type. However, their small size makes them difficult to identify,

especially since they likely correspond to a mixture of phases.

Journal Pre-proof

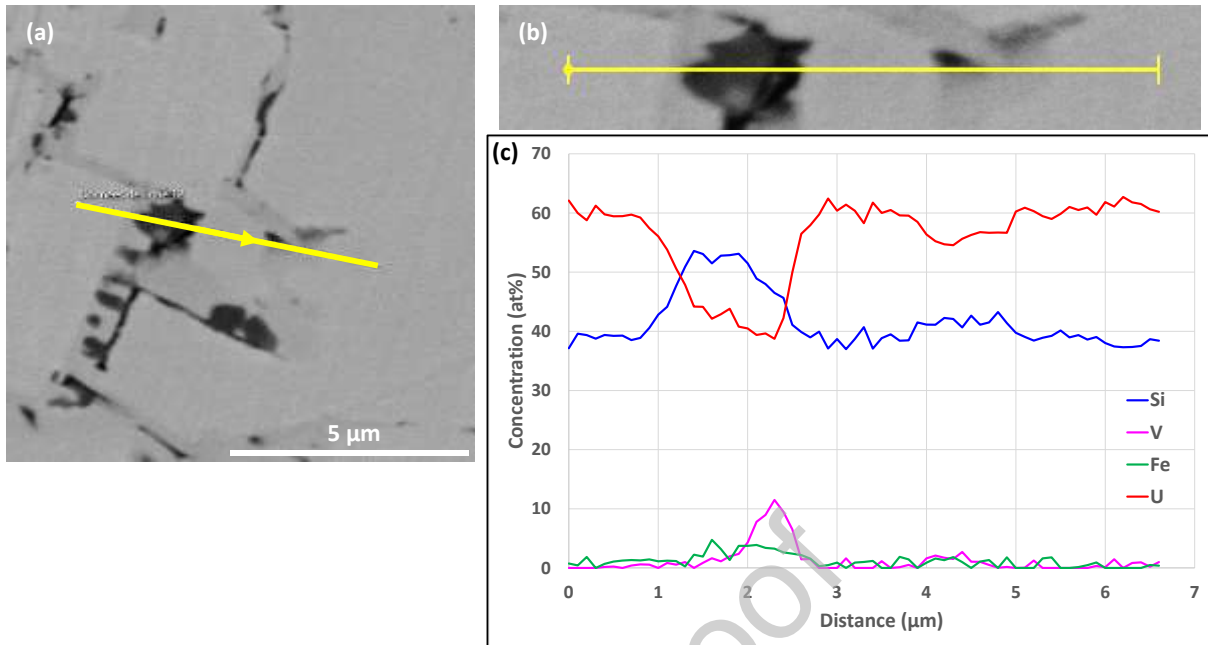


Figure 8: EDS analysis through a dark grey secondary phase in a particle from batch C of U_3Si_2 atomized powder: (a) (b) electron micrographs (SEM, BSE mode) indicating the position of the line-scan (yellow lines), (c) corresponding composition profiles.

3.4 EBSD ANALYSES

The purpose of the EBSD analyses was twofold:

- Firstly, to study the microstructure of the U_3Si_2 major phase (size and shape of grains, possible preferential orientations, etc.),
- Secondly, to get additional information about the minor phases.

To meet the first objective, large EBSD maps including at least a dozen of particles were acquired, considering only the U_3Si_2 phase for indexing the electron backscatter diffraction patterns (EBSPs). Similar results were obtained for the three batches. Figure 9 gives an example of map acquired on particles from batch A.

This map was acquired with a 0.4 μm step. Raw data were gently cleaned, to improve the detection of U_3Si_2 grain boundaries without eliminating all non-indexed pixels associated to defects (such as cracks, as visible when comparing Figures 9a and 9b) and minor phases present within grains. It is colorized according to the inverse pole figure for direction Z (IPF-Z) (the corresponding color code being displayed as inset to Figure 9b). Non-indexed pixels are displayed in black and grain boundaries with disorientations greater than 10° are drawn using black lines. The threshold angle of 10° chosen to define grain boundaries allows detecting almost all of them. This map shows that most of atomized particles comprise only a few grains. Some of them can even be single crystalline, as the one in a red dotted rectangle in Figure 9b. More rarely, smaller grains (with a size of about 10 μm) can be encountered, as in the case of the particle in a dotted white rectangle. It is worth noting that these small grains are mostly found in the scarce particles with a central porosity (this is the case for the particle in the white dotted box, where a relatively small and off-centred pore is pointed by a white arrow).

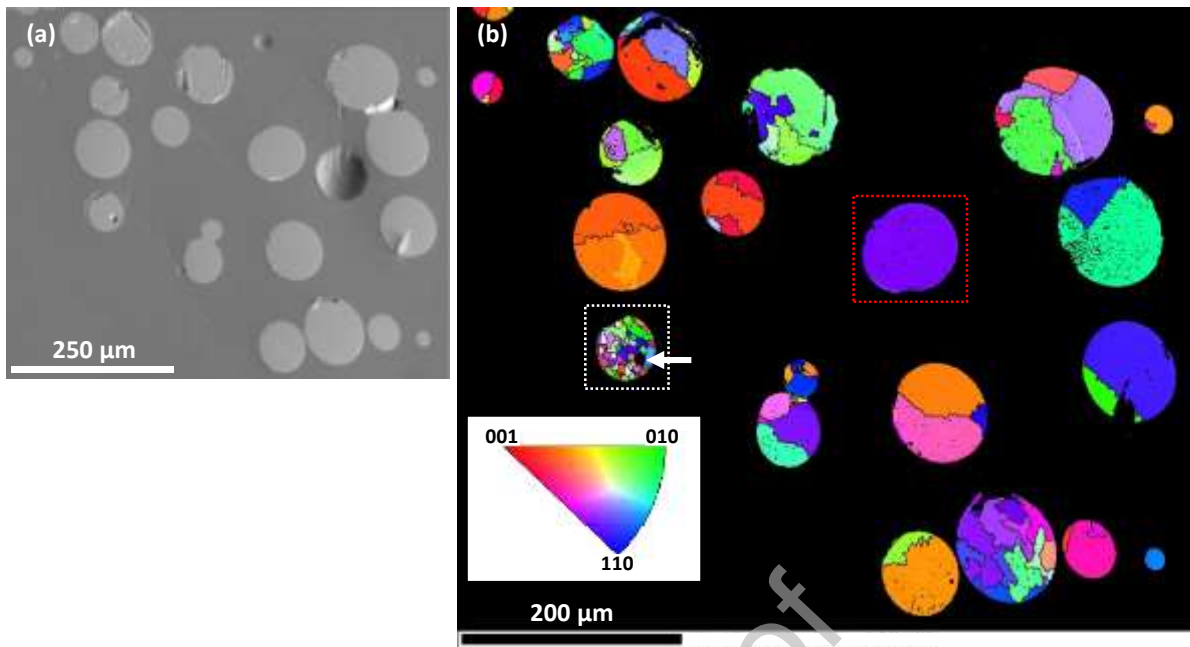


Figure 9: EBSD analysis of polished particles from batch A of atomized U_3Si_2 powder: (a) SEM image (secondary electron mode), (b) EBSD map colorized in IPF-Z + grain boundaries (black lines). Non-indexed pixels are coloured in black.

Local EBSD maps were acquired with a smaller step size (about $0.1 \mu\text{m}$) in particles from batches B and C, in order to confirm the presence of an $\text{U}_{20}\text{Si}_{16}\text{C}_3$ -like phase within the U_3Si_2 grains and get additional information about its characteristics. Figure 10 gathers such analyses for three particles with typical microstructures, *i.e.*, a particle with three U_3Si_2 grains (Figures 10a to 10c), a second particle with numerous smaller grains and a central porosity (Figures 10d to 10f) and finally a single crystalline one (Figures 10g to 10j). For each particle, three maps are presented (from left to right): pattern quality, grain orientation in IPF-Z and finally phase distribution with U_3Si_2 in yellow and $\text{U}_{20}\text{Si}_{16}\text{C}_3$ in blue. In Figures 10b and 10e, the IPF-Z maps are colorized considering both phases, whereas they are colorized only for one phase in Figures 10h (U_3Si_2 only) and 10i ($\text{U}_{20}\text{Si}_{16}\text{C}_3$ only). In all these maps, non-indexed pixels (coloured in black) have two main origins: first, physical defects such as cracks and holes and second, unidentified minor phases. These unknown phases correspond very probably to the dark ones in BSE images, as highlighted when comparing the enlarged area in Figure 10i with Figure 6f. The existence of orientation relationships between U_3Si_2 and $\text{U}_{20}\text{Si}_{16}\text{C}_3$ is obvious, when looking at the IPF-Z maps of particles 1 (Figure 10b) and 3 (Figures 10h and 10i). Indeed, in particle 1, the $\text{U}_{20}\text{Si}_{16}\text{C}_3$ veins have the same orientation within a given U_3Si_2 grain and that orientation changes from one grain to the other. In the case of particle 3, which is single crystalline, only one orientation is also evidenced for the $\text{U}_{20}\text{Si}_{16}\text{C}_3$ phase. The following orientation relationship can be deduced from this map: $[001] \text{ U}_3\text{Si}_2 // [0001] \text{ U}_{20}\text{Si}_{16}\text{C}_3$. Such relationship was checked in several other particles.

Approximate surface fractions of 9 % and 20 % of $\text{U}_{20}\text{Si}_{16}\text{C}_3$ -like phase were determined for batches B and C respectively, on the basis of the analysis of several particles per batch. These values are not far from those determined in mass fraction by Rietveld refinement of XRD data, knowing that U_3Si_2 and $\text{U}_{20}\text{Si}_{16}\text{C}_3$ have close densities [33].

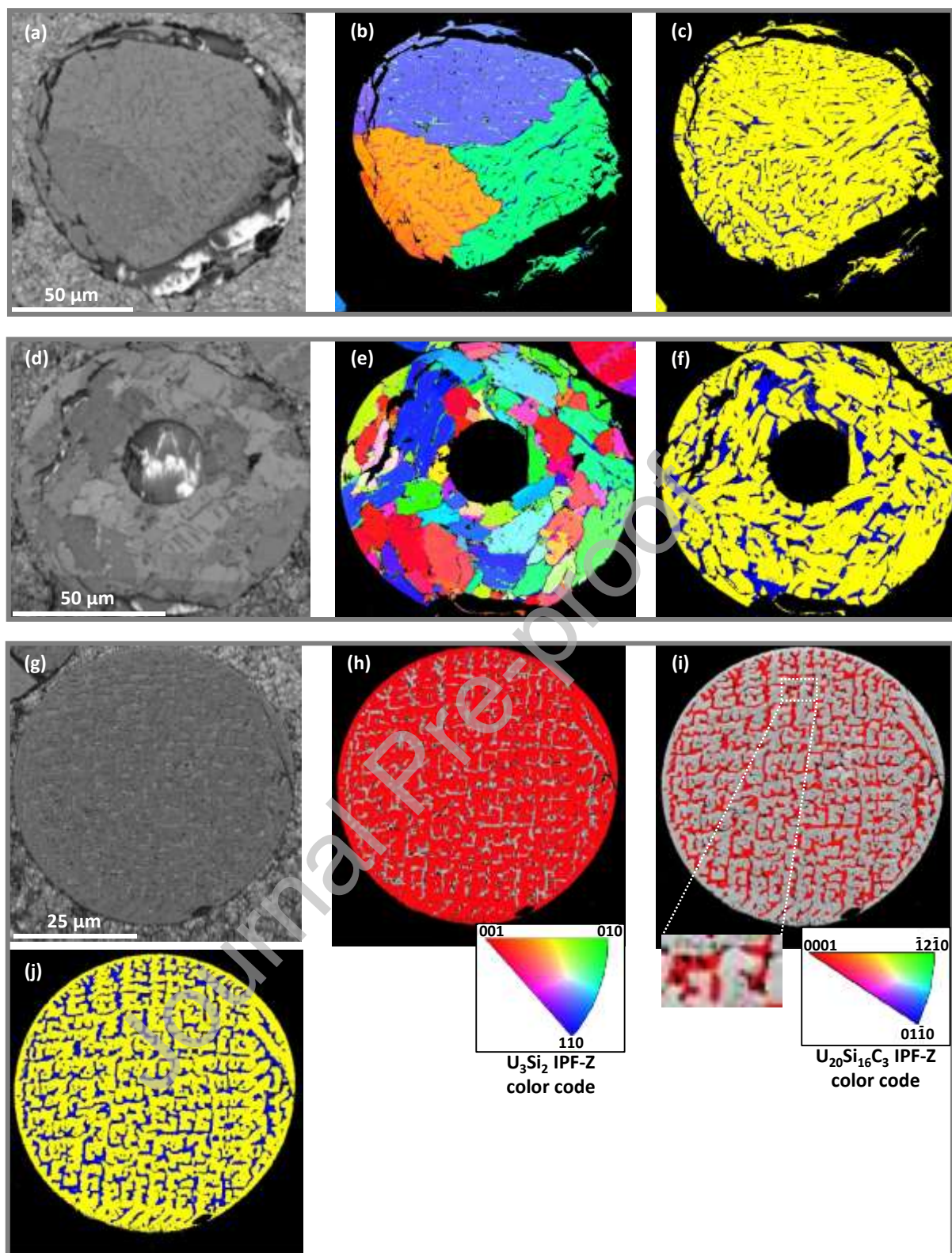


Figure 10: EBSD analysis of polished particles from batches B and C of atomized U₃Si₂ particles – Particle 1 (batch B) shown (a) in pattern quality, (b) in IPF-Z for U₃Si₂ + U₂₀Si₁₆C₃, (c) in phase distribution – Particle 2 (batch C) shown (d) in pattern quality, (e) in IPF-Z for U₃Si₂ + U₂₀Si₁₆C₃, (f) in phase distribution - Particle 3 (batch C) shown (g) in pattern quality, (h) in IPF-Z for U₃Si₂, (i) in IPF-Z for U₂₀Si₁₆C₃, (j) in phase distribution. In phase distribution maps, U₃Si₂ appears in yellow and U₂₀Si₁₆C₃ in blue. Non-indexed pixels are in black.

Finally, some local maps were acquired with an even smaller step size (about 80 nm) and the EBSPs were saved for all the non-indexed pixels. These data were used to progress on the identification of the unindexed minor phases (dark phase(s) on electronic images). Different binary and ternary silicides unit cells (such as those of U_3Si_5 , USi_2 or $U_2V_3Si_4$ (see section 3.5) for example were tested since their elemental composition was consistent with EDS characterizations. These tests showed that at least two different phases had to be taken into account to index these areas. However, the agreement between the experimental diffraction patterns and the theoretical ones was not good enough to allow their unambiguous identification.

To get additional information on these unidentified minor phases, TEM lamellas were prepared by FIB and studied by STEM + EDS.

3.5 TEM LAMELLAS PREPARATION AND EXAMINATION

The aim of the complementary analyses mainly performed by STEM + EDS was:

- first, to analyze the composition of minor phases present in the core of the atomized particles, with a better spatial resolution than that achievable by SEM,
- second, to identify from their composition the nature of phases located at the extreme surface of the particles (where they form a network of very fine lamellas).

To facilitate the STEM + EDS characterizations, particles from batch C were selected, as they present thicker veins of secondary phases than those from the other two batches. Two lamellas were prepared by FIB milling, using a classical lift-out method: one from a polished section of a particle, in an area where veins of minor phases were present, and the other directly from the outer surface of an as-atomized unpolished particle. In the latter case, a thicker than usual Pt-base layer was deposited before milling to protect this surface from a too quick thinning.

Figure 11a shows a general view of the first lamella. Details darker than the U_3Si_2 matrix are visible. The red dotted square drawn on this figure is observed at higher magnification in Figure 11b. The latter corresponds to a STEM-HAADF image and presents composition contrasts. According to grey levels, at least three types of phases are present: U_3Si_2 in light grey on the right side of the image, a medium grey phase which forms a partial triangle in the central part, and dark particles (with a size of the order of one to a few hundred nanometers) located within this medium grey area. Thanks to EDS analyses performed in a part of this area (green-boxed in Figure 11b), it was possible to precise the elemental composition of these different phases. Uranium and silicon maps (Figures 11d and 11e) clearly show that they do not have the same Si content. Furthermore, the darker phases contain other elements that is: Fe, V and Mo. Iron is concentrated in the particles with the higher Si content, while V and Mo are co-localized in other dark particles with a lower Si amount. Quantified data calculated from four positions in the map (defined in Figure 11i) are gathered in Figure 11j. Position 1 undoubtedly corresponds to the U_3Si_2 matrix. Position 4 is characterized by a bit higher Si content (about 47 at%). Taking into account an uncertainty of a few at% on this value (linked at least partly to thickness variations in the lamella which are not measured and thus not considered), it seems reasonable to assume that it corresponds to the $U_{20}Si_{16}C_3$ -like phase which was previously identified in the present work thanks to XRD, EDS at SEM scale and EBSD. Positions 2 and 3 correspond to uranium silicides containing different metallic impurities. In the case of position 2, the only detected impurity is iron and the composition of the phase is given approximately by the following empirical formula: $UFe_{0.2}Si_{1.8}$. It could therefore be attributed to a solid solution of iron in USi_2 , as expected from the ternary U-Fe-Si phase diagram [34].

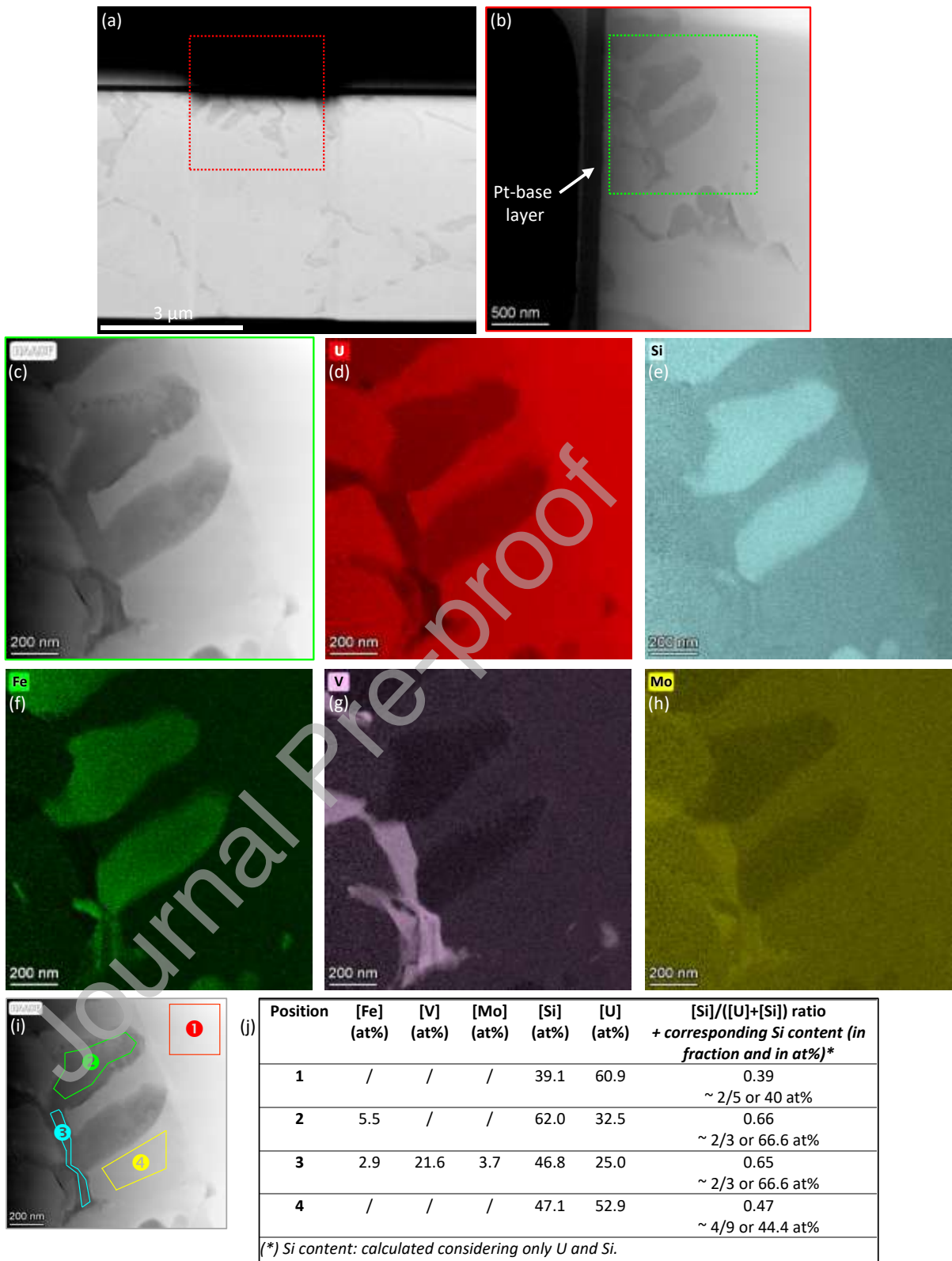


Figure 11: STEM + EDS analysis of a FIB lamella taken from a polished section of a particle from batch C of atomized U_3Si_2 powder - (a) (b) general views of the lamella respectively taken by SEM (BSE mode) and STEM (HAADF mode), (c) STEM-HAADF image of the area analysed by EDS, (d) (e) (f) (g) (h) X-ray maps for U (in red), Si (in light blue), Fe (in green), V (in light purple) and Mo (in yellow), (i) location of parts of the map for which corresponding quantitative results are given in (j).

In the case of position 3, the main metallic impurity is V, but some Fe and Mo are also detected. The elemental composition of this zone as given by EDS is 25U-28M-47Si (in at%, with M = V + Fe + Mo). This composition is not far from the $U_2V_3Si_4$ phase (which would be written here $U_2M_3Si_4$) proposed by Noël and Rogl [35]. These results are consistent with those obtained by EDS at SEM scale (cf. Figures 5 and 8): they confirm the quasi-systematic presence of Fe and/or V in minor dark phases, with partitions of these elements linked to the Si distribution. They also show that other metallic impurities can come into play more locally and rarely, such as Mo here.

This lamella was also studied by electron diffraction. As an example, Figure 12b shows a diffraction pattern obtained from the selected area circled in red in Figure 12a. This area corresponds to position 4 in Figure 11i, which is characterized by a $[Si]/[U]+[Si]$ close to 4/9. The pattern is typical of a single crystal. It was indexed as an $U_{20}Si_{16}C_3$ -like phase, with a [-221] zone axis (Figure 12c). Note that its orientation is not fully perfect (due to tilt limitations encountered with the specimen holder), because the intensity of symmetrical diffraction spots (by reference to the (000) position) is not identical.

Electron diffraction coupled with EDS analyses therefore confirmed the presence of an $U_{20}Si_{16}C_3$ -like phase in this lamella. The presence of U_3Si_2 was also checked easily but the diffraction patterns obtained in the minor phases containing metallic impurities could not be indexed accurately when testing various binary and ternary uranium silicides structures.

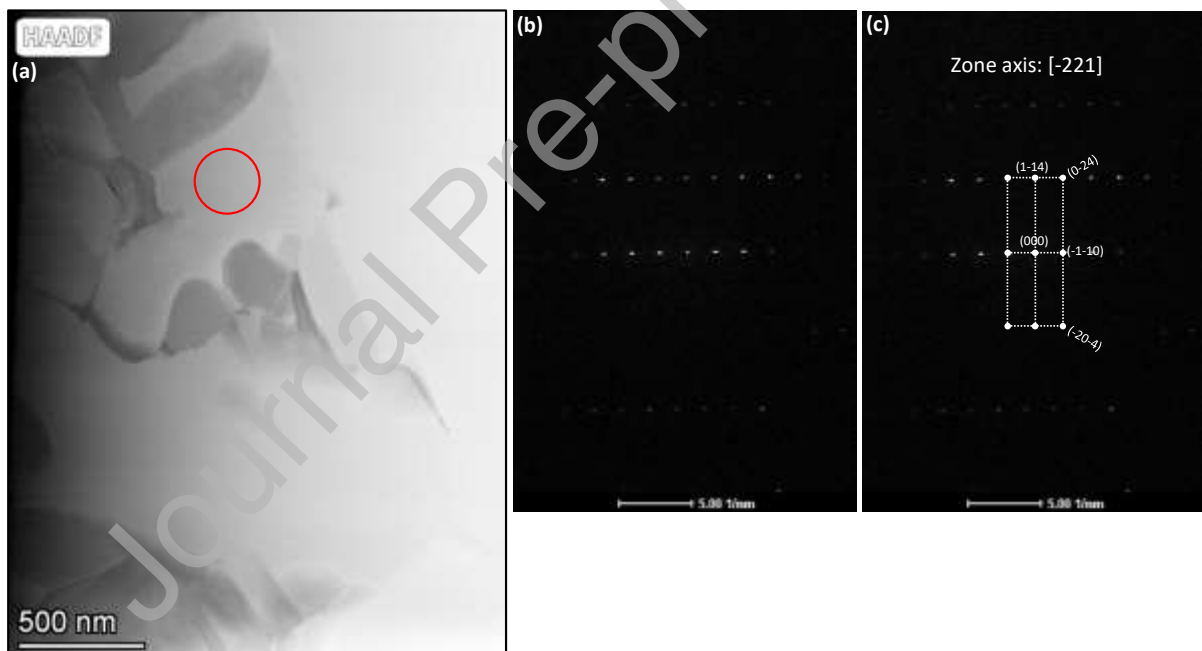


Figure 12: STEM + electron diffraction analysis of a FIB lamella taken from a polished section of a particle from batch C of atomized U_3Si_2 powder - (a) STEM-HAADF image of the area under study, (b) electron diffraction pattern obtained in the area circled in red in (a), (c) indexation of the pattern shown in (b) considering a $U_{20}Si_{16}C_3$ -like unit cell.

Figure 13 summarizes the results obtained on the lamella removed from the outer surface of the un-polished atomized particle. As illustrated by Figures 13c and 13d, a layer of about 100 nm in thickness is present at its surface and comprises nano-crystallized phases.

X-ray maps (Figures 13e to 13h) clearly show that oxidized islets are present at that surface and are depleted in Si. As a consequence, a Si enrichment is observed around and below these islets.

Some vanadium is also detected very locally at some interfaces. Semi-quantitative compositions (with no absorption corrections) associated to the areas drawn in Figure 13i are presented in Figure 13j. When moving from the surface to the core of the particle, the following areas are encountered:

- Area 1: it corresponds to an oxidized islet, its Si content is very low and its O/U ratio is higher than 3. This ratio is very probably over-estimated, as oxygen is present on the whole surface of the lamella. It could be representative of an UO_2 layer that became a bit hyper-stoichiometric during the storage of the powder in air [36]. Its thickness is so small (50 nm at the most) and it is so discontinuous that it was not detected by XRD and was not observed either by SEM on polished sections or on fractured particles.
- Area 2: this area surrounds the oxidized islets and contains only Si and U. Its composition is close to USi_2 .
- Area 3: this area is very thin (from 15 to 35 nm, approximatively) and seems to correspond to a transition layer between areas 2 and 4. Its composition is close to USi .
- Area 4: this area corresponds to the U_3Si_2 matrix (with a slight over-estimation of the Si content).

All these features seem to be attributable to a slight oxidation of the surface of the particle that probably occurred when it was a molten droplet (highly reactive with oxygen traces present in the atomizer chamber). This superficial oxidation induced local silicon segregation processes that led to the formation of silicides richer in Si than the U_3Si_2 core of the particles. The size of these superficial Si enriched areas was too small to permit their study by selected area electron diffraction.

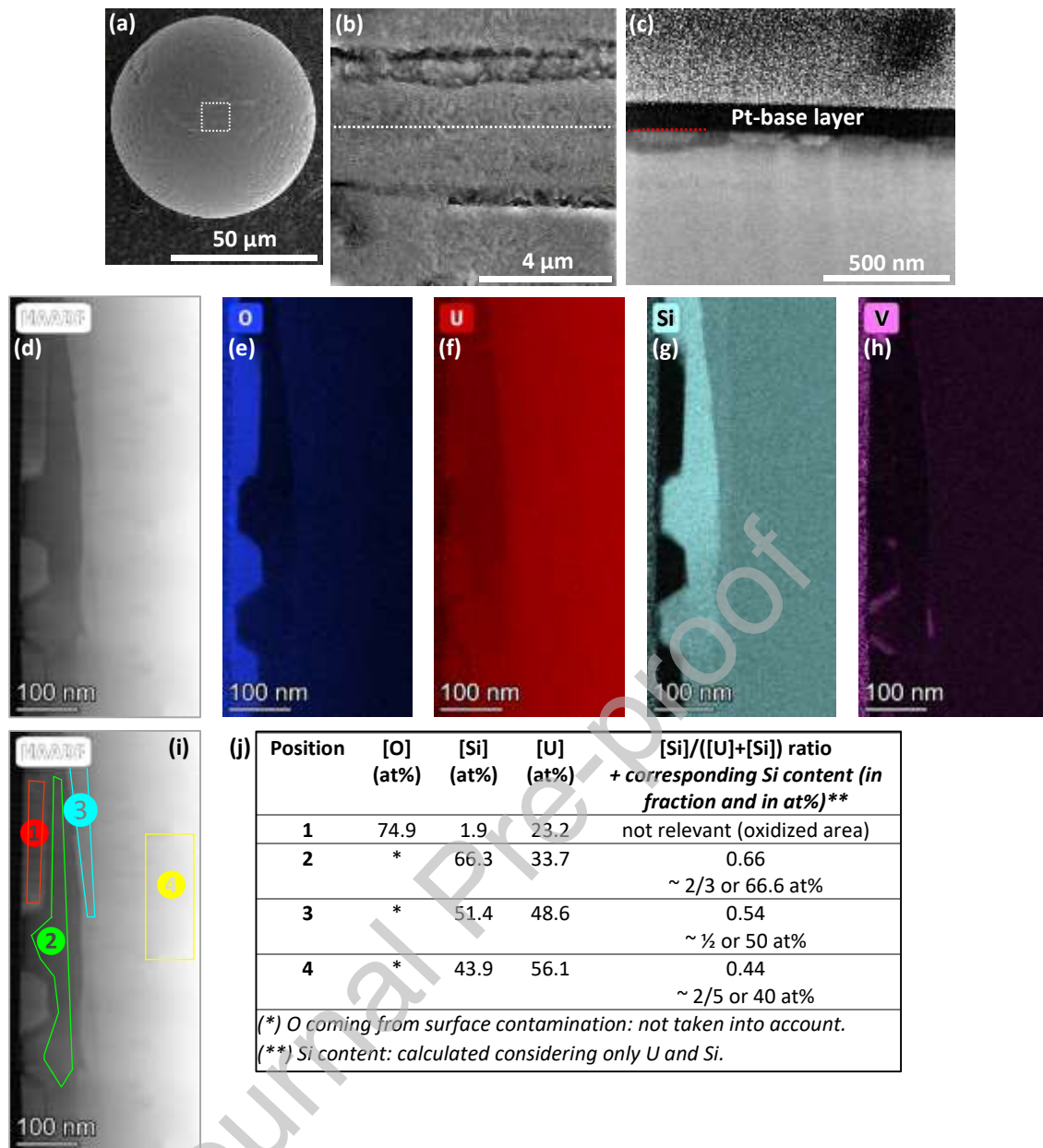


Figure 13: STEM + EDS analysis of a FIB lamella taken from the surface of a particle from batch C of atomized U_3Si_2 powder - (a) (b) SEM images (secondary electrons) of the surface of the un-polished particle before its milling (the white dotted box in (a) corresponds to the area shown in (b) and the white dotted line in (b) corresponds approximately to the position where the lamella was taken), (c) STEM (HAADF mode) image of a thinned part of the lamella including the superficial part of the particle (the position of its surface being indicated by the red dotted line), (d) STEM-HAADF image of the area analysed by EDS, (e) (f) (g) (h) X-ray maps for O (in deep blue), U (in red), Si (in light blue) and V (in light purple), (i) location of parts of the map for which corresponding quantitative results are given in (j).

4. DISCUSSION

This discussion is mainly devoted to the minor phases present in the core and at the external surface of U_3Si_2 atomized powders. A summary of what is known (or not) about these phases, based on this work, is done first. Two groups of “minor” phases are then distinguished, depending on whether their origin may be mainly linked to the atomization process or to the purity of the raw uranium. Microstructural features of atomized particles are also considered.

4.1 SUMMARY OF MAIN RESULTS CONCERNING MINOR PHASES CHARACTERISTICS

Table 3 summarizes the main information about the characteristics of the minor phases drawn from the analysis of powders from the three powder batches by XRD, EDS (at micrometer (SEM) and nanometer (TEM) scales), EBSD and electron diffraction.

Batch A, which is nearly stoichiometric, contains a very small amount of minor phases. These latter probably crystallize after U_3Si_2 in the inter-dendritic spaces, from a liquid enriched with Si and segregated impurities. Because of their very small size, they were characterized only partly. According to EDS (performed at SEM scale), they contain metallic elements such as V, Fe and Al. These results are consistent with chemical analyses given in Table 1, as Fe and Al are the main metallic impurities present in the three batches. The V content was not measured in these batches but was determined in the raw uranium batch, in which its concentration reached 0.21 wt%. One cannot exclude that light elements, and especially carbon (418 ppm in this batch), could also enter in the composition of certain of these phases.

Atomized particles from batches B and C contain a significant amount of an $\text{U}_{20}\text{Si}_{16}\text{C}_3$ -like phase. As already mentioned, the carbon content of this phase was not measured by EDS and could be lower than that given in its formula. Indeed, this phase is crystallographically very close to U_5Si_4 , which has the same Si/U ratio and is supposed to be stabilized by carbon traces [27] [28]. It is also worth noting that the carbon content of batch C is about eight times higher than that of batch B (1190 ppm instead of 150 ppm). This amount, coupled with a higher silicon hyper-stoichiometry and also to very probable micro-segregation effects, seems to be clearly favorable to the formation of this phase.

Metallic impurities are involved in the formation process of other minor phases located within $\text{U}_{20}\text{Si}_{16}\text{C}_3$ -like veins. Thanks to local EDS analyses performed at nanometer scale on a TEM lamella, two types of phases were evidenced:

- a first one with a significantly higher Si content than U_3Si_2 , in which the major impurity is Fe (empirical formula determined locally would be close to $\text{UFe}_{0.2}\text{Si}_{1.8}$),
- a second one with a slightly higher Si content than U_3Si_2 , in which the major impurity is V (empirical formula determined locally would be close to $\text{U}_2\text{M}_3\text{Si}_4$, with M = metallic impurities).

Table 3: Summary of main information about minor phases present in the three batches of atomized U₃Si₂ powders, according to XRD, EDS, EBSD and electron diffraction analyses. « Dark grey » and « light grey » designations refer to the contrast of the phases in SEM images obtained in BSE mode.

	Batch A	Batches B and C
XRD	No minor phase identified (few very small diffraction peaks remaining unindexed)	<ul style="list-style-type: none"> - Identification of an U₂₀Si₁₆C₃-like phase - Mass fraction of this phase (determined by Rietveld refinement): <ul style="list-style-type: none"> o 10(5) wt% in batch B o 21(5) wt% in batch C - Few very small diffraction peaks remaining unindexed
EDS	<p>At SEM scale:</p> <p>Dark grey minor phase(s) with:</p> <ul style="list-style-type: none"> - Frequently higher Si content than in U₃Si₂ - Metallic impurities (mainly V and Fe) 	<p>At SEM + TEM scales:</p> <ul style="list-style-type: none"> - Light grey phases: <ul style="list-style-type: none"> o Confirmation of a [Si]/[U]+[Si] ratio close to 4/9, corresponding to that encountered in an U₂₀Si₁₆C₃-like phase o C content : not determined - Dark grey phases : <ul style="list-style-type: none"> o Metallic impurities (mainly V and Fe) heterogeneously distributed o Fe: seems to be mainly present in a phase with a significantly higher Si content than U₃Si₂ (empirical formula determined locally: close to UFe_{0.2}Si_{1.8}) o V: seems to be mainly present in a phase with a slightly higher Si content than U₃Si₂ (empirical formula determined locally: close to U₂M₃Si₄, with M = metallic impurities) - At the extreme surface of the particles: <ul style="list-style-type: none"> o Oxidized islets (UO₂) o USi₂
EBSD	No results, because of the too small size of minor phases	<ul style="list-style-type: none"> - Light grey phases: <ul style="list-style-type: none"> o Confirmation of the identification of a U₂₀Si₁₆C₃-like phase, with the following approximate surface fractions in U₃Si₂ particles: 9 % for batch B and 20 % for batch C o Orientation relationship with U₃Si₂ matrix ([001] U₃Si₂ // [0001] U₂₀Si₁₆C₃) - Dark grey phases: <ul style="list-style-type: none"> o Not identified
Electron diffraction	Not studied by this method	<ul style="list-style-type: none"> - Light grey phases: <ul style="list-style-type: none"> o Confirmation of the presence of an U₂₀Si₁₆C₃-like phase - Dark grey phases: <ul style="list-style-type: none"> o Not identified

These analyses are consistent with those performed at the micrometer scale in batches B and C. They should also be representative (at least partly) of the phases present in batch A. However, they are probably not fully representative of all particles since variations in impurities local content are likely to occur within particles, depending on their size and solidification rate (which will influence segregation phenomena). Light elements and especially carbon should also be analyzed accurately to get additional information about the elemental composition of the minor phases. Indeed, various « ternary » compounds stabilized by impurities could be encountered, as proposed by Ulrich *et al.* on the basis of high temperature time-of-flight neutron diffraction coupled with *ab initio* calculations [28].

A very superficial oxidation of the particles, inducing a local segregation of Si must be also noticed. The extent of this surface oxidation is likely to vary from batch to batch, depending on the synthesis and storage conditions of the powders. Its thickness was found below 100 nm in the single local measurement reported in this work, made on one particle from batch C.

There are few elements of comparison of these results with other microstructural studies concerning U_3Si_2 atomized particles. In a paper published in 1997, Kim *et al.* reported the presence of USi and USi_2 phases at grain boundaries in a batch with 7.4 wt% Si [12]. The USi phase was identified by these authors only by EDS (with no structural confirmation). It could actually correspond to the $U_{20}Si_{16}C_3$ -like phase (with a U/Si ratio of 1.25) evidenced in the present work in batches B and C, thanks to several complementary tools (XRD, EDS, EBSD and electron diffraction). Concerning USi_2 , phases with a close composition were observed in the present work, either very locally in a TEM lamella taken from the surface of a particle or stabilized with iron inside the particles. Kim *et al.* also mentioned the presence of some α -U based on laboratory XRD data *i.e.*, without clear indication about its location within particles. No indication supporting the presence of such a phase could be found in the present work.

Finally, Jeong *et al.* indicated the presence of some UO_2 (detected by XRD) on the surface of as-atomized U_3Si_2 particles with 7.6 wt% Si [17] which is consistent with the present study.

4.2 ORIGIN OF MINOR PHASES

4.2.1 Expected phases, from U-Si phase diagram

On a basis of the U-Si binary diagram, as it is presented in handbooks [37], a composition corresponding to a Si hyper-stoichiometry of about 1 to 2 at% (as it the case for batches B and C) compared to the U_3Si_2 nominal composition (40 at% Si) corresponds to an hypo-eutectic alloy (U_3Si_2 + USi eutectic composition: 46 at% Si). In such an alloy, the U_3Si_2 phase solidifies first, as primary large crystals [38]. The remaining liquid is then enriched in Si and solidifies in a second step, in the form of an eutectic microstructure *i.e.*, a mixture of U_3Si_2 and « USi » [38] or more exactly $U_{34}Si_{34.5}$ [28].

After syntheses by arc melting of ingots also slightly hyper-stoichiometric in silicon, the $U_{34}Si_{34.5}$ phase was effectively observed, as expected from this diagram [8]. This phase was also identified in U_3Si_2 pellets manufactured by powder metallurgy, from crushed arc-melted ingots with 7.5 wt% Si [7]. Likewise, the U_5Si_4 phase was detected in small amounts in some of these pellets [39]. This latter phase was presented as a potential equilibrium one (formed by peritectic reaction) in a revised U-Si phase diagram, proposed by Ulrich *et al.* [28]. However, these authors finally assessed that it was probably metastable or stabilized by one or more impurities, such as oxygen or carbon. In the same way, other phases may be metastable in the U-Si system. Their formation could be linked to high cooling rates and/or impurities. It is the case, for example, of the U_8Si_8X phase (where X refers to light elements) encountered in some arc-melted ingots [8].

Atomized particles undergo very high cooling rates evaluated to about 10^4 K.s⁻¹ [40] instead of

about ten times less for arc melting [41]. Moreover, they seem to be systematically polluted by some carbon coming from the atomization process and some metallic impurities coming from the raw uranium. For these different reasons, they are very probably out of equilibrium.

4.2.2 Minor phases linked to the atomization process

Among the phases listed in Table 3, some of them are likely to be quite systematically encountered in U_3Si_2 atomized powder batches:

- the $\text{U}_{20}\text{Si}_{16}\text{C}_3$ -like phase, observed in the core of the particles from batches B and C, which are hyper-stoichiometric in Si up to 1 to 2 at%,
- the UO_2 islets observed at their surface and the related silicides located just close to these islets.

The formation of an $\text{U}_{20}\text{Si}_{16}\text{C}_3$ -like phase, instead of the $\text{U}_{34}\text{Si}_{34.5}$ equilibrium phase, is very probably due to the presence of carbon in the $\text{U} + \text{Si}$ liquid which comes from graphite parts present in the induction melting furnace. Such carbon contamination was also reported for as-atomized U-Mo powders manufactured by KAERI, leading to carbon-rich secondary phases ($\text{U}(\text{C},\text{O})$) [42].

It is interesting to compare this result with the observation of some U_5Si_4 phase, identified by XRD and EDS in U_3Si_2 sintered pellets. The U_5Si_4 amount was low (a few wt%) even in pellets containing up to 3500 ppm of carbon [39] compared to 1190 ppm, in present batch C. The high carbon pollution of sintered pellets was attributed to organic lubricant and binder used during milling and pressing steps of U_3Si_2 (previously synthesized by arc-melting) and also to the graphite crucible used for sintering [7]. $\text{U}_{20}\text{Si}_{16}\text{C}_3$ and U_5Si_4 have close crystallographic characteristics and can be confused with each other, especially when analyzing XRD diffraction data in which they only correspond to few minor peaks. Assuming that both phases are almost the same (or could even coexist) and come from carbon pollution of U_3Si_2 , it has to be noted that this pollution did not occur at the same stages of the two manufacturing processes. Indeed, in centrifugal atomization, it came into play during the synthesis of the U_3Si_2 phase by fusion-solidification, which was very probably associated to strong micro-segregation effects of silicon and impurities in the remaining liquid (considering the high cooling rate of droplets), whereas in powder metallurgy, U-Si phases were already formed (except perhaps some U_3Si) when they became in contact with carbon and only solid-state reactions governed by slow diffusion processes could then occur.

This difference could explain why an $\text{U}_{20}\text{Si}_{16}\text{C}_3$ -like phase forms in atomized particles, in significant quantity. It appears likely that three conditions should be full-filled simultaneously: (i) the presence of carbon as an impurity in the melt, (ii) a sufficient silicon hyper-stoichiometry, (iii) a high cooling rate favoring the micro-segregation of carbon and silicon. Some flexibility should exist on these three conditions. In the present work, they would be met in batches B and C but perhaps not in batch A because it is almost stoichiometric in Si. The presence in this latter batch of a very small amount of the $\text{U}_{20}\text{Si}_{16}\text{C}_3$ -like phase cannot be fully excluded, even if none of the characterization techniques implemented on this sample made it possible to identify it.

The U_3Si_2 fuels used in research reactors are synthesized from ^{235}U low enriched uranium (LEU) with a higher purity than the ^{235}U depleted uranium (DU) used to obtain the three batches studied in the present work. This higher level of purity mainly concerns metallic impurities (such as Fe, V, Al...) but light elements (C and O, mainly) contents are almost the same between DU and LEU atomized particles. So, the most abundant minor phase *i.e.*, the $\text{U}_{20}\text{Si}_{16}\text{C}_3$ -like phase evidenced in this study should also be present in LEU particles intended to be irradiated in a research reactor. The impact of the presence of this phase on the irradiation behaviour of U_3Si_2 particles is unknown so far to the best of our knowledge.

A slight superficial oxidation of metallic particles produced by atomization is reported in numerous studies (see e.g. [43] [44]). It is directly linked to the very high reactivity of metals or alloys

at high temperatures towards oxygen traces present in atomization devices. According to the Ellingham diagrams, at temperatures comprised between 500 and 2500 K, uranium is more oxidizable than silicon and uranium silicides [45]. This thermodynamic property can explain why only uranium oxide (UO_2) is formed in presence of oxygen traces and why silicon is then rejected, inducing a local enrichment in this element. The examinations performed locally by STEM + EDS on a TEM lamella showed that a USi_2 phase seems to form but one cannot exclude that other silicides could also appear. According to studies performed on tailored oxidized U-Mo particles [46] an outer UO_2 layer at the surface of the U_3Si_2 particles could have a slight protective effect against interactions with the Al matrix. However, this effect will probably be limited taking into account the discontinuity and the very low thickness of this layer. The presence of different silicides (other than U_3Si_2) at the periphery of the particles could also slightly impact the interaction processes with Al. Upcoming post-irradiation examinations on the KIMQI plates [14] are likely to provide information about such possible effects.

4.2.3 Minor phases linked to the purity of the raw uranium

Thanks to EDS analyses (especially those performed at nanometer scale), minor phases containing metallic elements (mainly V and Fe) were evidenced. As indicated in Table 1, the three batches contain about 0.1 wt% Al and 0.1 wt% Fe, as major impurities coming from the raw uranium batch. Their V content was not determined but it was measured in the raw U batch, where it reached 0.21 wt%.

As a line compound, U_3Si_2 solidifies first extremely fast (its equilibrium temperature of solidification being 1938 K). The remaining liquid, located in inter-dendritic spaces, is then enriched in Si and also in segregated impurities (*i.e.*, carbon mainly coming from the crucible and metallic elements coming from the raw uranium batch). In a second step, this liquid solidifies to form an $\text{U}_{20}\text{Si}_{16}\text{C}_3$ -like phase (its solidification temperature is about 1870 K [24] but supercooling is likely to occur), perhaps via a peritectic reaction as proposed by Ulrich *et al.* for U_5Si_4 [28].

The last remaining pockets of liquid, located within the $\text{U}_{20}\text{Si}_{16}\text{C}_3$ -like phase veins, then give rise to at least two other types of phases which solidify at a very last step and in which a partition of the remaining Si and of metallic impurities occurs: Fe seems to be incorporated in solid solution in a USi_2 -like phase ($\text{UFe}_{0.2}\text{Si}_{1.8}$), while V forms a “ternary” silicide (with a $\text{U}_3\text{M}_4\text{Si}_4$ approximate formula). These behaviors are consistent with the absence of solubility of Fe and V in U_3Si_2 as indicated in the available descriptions of the U-Fe-Si and U-V-Si ternary systems [34] [35]. From a more general point of view, the presence of other minor phases associated to other metallic impurities (such as Al, Cr, Mo ...) in U_3Si_2 atomized particles should not be excluded, depending on the purity of the raw uranium batch and local segregation effects. In LEU fuels which are made with raw uranium of a better purity than that used to synthesize the DU powders studied in the present work, the amount of “ternary” silicides including metallic impurities is expected to be significantly lower.

4.3 MICROSTRUCTURAL CHARACTERISTICS OF ATOMIZED PARTICLES

Microstructural features evidenced in atomized particles are very likely the result of (i) first, a dendritic solidification of the U_3Si_2 compound accompanied by a silicon and impurities enrichment of the remaining liquid, (ii) second, the solidification of secondary phases in inter-dendritic spaces.

Of course, the solidification rate as well as the sharpness and direction of the thermal gradient influence the morphology of the dendrites. That is why there are differences between arc-melted ingots (for which a strong directional thermal gradient is imposed by the cooled hearth of the furnace during their solidification) and atomized particles (subjected to radial gradients and to much faster cooling rates). In ingots, U_3Si_2 grains are large (often millimetric) with a relatively marked columnar morphology [8], while in atomized particles, grain size is limited to a few tens of

micrometers and the grain shape is not columnar. Monocrystalline particles can also be encountered, as often observed in comminuted U_3Si_2 powders [8]. These characteristics are quite different from those observed in U-Mo atomized particles, where grains are significantly smaller, with a few microns typical size, and commonly columnar [18]. This difference could be due to the much higher melting point of U_3Si_2 (1938 K) compared to that of U-Mo alloys (about 1430 K) and to its congruent solidification which seems to favour the crystallization of coarse dendrites, even at high cooling rates.

The $U_{20}Si_{16}C_3$ -like phase appears in a second step and forms oriented veins inside the U_3Si_2 grains. The formation of geometrical patterns of secondary phases was also assessed in U_3Si_2 arc-melted ingots containing $U_3Si_{34.5}$ and U_8Si_8X minor phases and was attributed to a solidification mechanism of a eutectic defined by the quadratic cell of the U_3Si_2 phase [8]. A similar mechanism seems to come into play in atomized particles, although it is uncertain if the $U_{20}Si_{16}C_3$ -like phase forms a eutectic with U_3Si_2 . Indeed, a peritectic reaction seems to be more probable, on the basis of the hypothetical binary phase diagram proposed by Ulrich *et al.* where an U_5Si_4 phase (very close to $U_{20}Si_{16}C_3$) is considered [28]. In-pile experiments should allow to evaluate whether this peculiar microstructure could affect the behavior of U_3Si_2 particles under irradiation, knowing that this latter phase becomes amorphous very quickly at irradiation temperatures encountered in MTRs [47] [48].

5. CONCLUSION

U_3Si_2 atomized particles are currently studied as an alternative to comminuted powders for the manufacturing of dispersion fuels for MTRs. This work aimed at supplementing the partial microstructural characterization results available on this material. To evaluate the impact of slight Si over-stoichiometries (recommended to ensure a satisfactory behaviour under irradiation), three batches were examined: a nearly stoichiometric batch (batch A) and two hyper-stoichiometric ones (batches B and C, with a Si excess of 1.6 and 1.9 at% respectively). It is important to note that the depleted uranium raw material used to synthesize these powders contained some metallic impurities and that carbon was also present in the final products, especially in batch C.

The atomized particles are almost perfectly spherical with a monomodal size distribution for batches A and C around respective mean ECD values of 55 μm and 75 μm . In the case of batch B, a more spread size distribution was observed and the particles are a bit less spherical, due to instabilities during the atomization process. Most of atomized particles comprise only a few grains and some of them are even single crystalline. Moreover, particles systematically contain secondary phases that form veins within U_3Si_2 grains. In batch A, these veins are too thin to be analysed by EDS without an important contribution of the surrounding U_3Si_2 matrix. Despite this limitation, it was possible to assess that they often contain more Si than U_3Si_2 and/or also some metallic elements (V and Fe, mainly). In batches B and C, the presence of an $U_{20}Si_{16}C_3$ -like phase was clearly assessed by XRD and EDS (with the following mass fractions estimated by Rietveld refinement of XRD data: 10(5) wt% for batch B and 21(5) wt% for batch C) and confirmed by electron diffraction. At least two other minor silicide phases containing metallic elements (Fe or V, mainly) are also evidenced. Finally, the examination of a TEM lamella taken from the surface of a particle from batch C showed that its surface presents oxidized islets with a thickness of about 50 nm at most. This superficial oxidation induces a local silicon segregation that leads to the formation of silicide(s) richer in Si than the U_3Si_2 core.

All these results point out a major role of impurities in the formation of secondary phases, their nature and morphology being strongly linked to segregation phenomena. Some of them are likely to be encountered in almost all U_3Si_2 powder batches, as their formation seems to be linked to the atomization process. The first and most abundant one is an $U_{20}Si_{16}C_3$ -like phase, present in the core of the particles. It very likely forms after the U_3Si_2 primary phase, from a liquid enriched in Si and C. It

is expected to be present also in particles made with high purity uranium, since C mainly comes from the induction furnace, and its behavior under irradiation should be assessed. The others are located at the surface of the particles and correspond to UO_2 islets, which are surrounded by uranium silicide(s) richer in Si than U_3Si_2 . Depending on their thickness and continuity, these superficial particularities may have an impact on the interaction processes between the U_3Si_2 particles and the Al matrix that occur under irradiation in an $\text{U}_3\text{Si}_2/\text{Al}$ dispersed fuel.

The other minor phases are “ternary” silicides containing metallic impurities (such as Fe and V) coming from the uranium batch used to synthesize the U_3Si_2 powder. Their presence is thus directly linked to the purity of uranium (that of silicon being generally very high). They were not fully identified in this study. To this end, supplementary characterizations and elemental analyses should be performed by TEM and electron diffraction, as well as by STEM + EDS on several particles per batch. Electron energy loss spectroscopy could also be used to detect light elements in minor phases, and especially carbon in the $\text{U}_{20}\text{Si}_{16}\text{C}_3$ -like phase.

It would also be interesting to anneal some particles and then characterize them in order to evaluate the stability of minor phases, some of them being probably out of equilibrium.

However, despite the interest of this complementary work, it would be wise to study another batch of atomized U_3Si_2 powder with a higher degree of purity (less metallic impurities in raw uranium and perhaps less carbon contamination).

Acknowledgements:

This work was supported by the KAERI Institutional Program (Project No. 522210-22).

J. Gousseau and N. Tarisien, from CEA Cadarache, are warmly thanked for performing the preparation and characterization of the samples by XRD, SEM, EDS and EBSD. M. Cabié, from University of Marseille is also thanked for the preparation of TEM lamellas by FIB milling.

CREDIT AUTHORSHIP CONTRIBUTION STATEMENT

X. Iltis: Investigation, Methodology, Writing - original draft. **J. Havette:** Investigation, Methodology, Writing – original draft. **V. Klosek:** Investigation, Methodology. **C. Onofri:** Investigation, Methodology. **K.H. Lee:** Project administration, Supervision, Writing - review & editing. **J.H. Kim:** Supervision, Writing - review & editing. **Y.J. Jeong:** Supervision, Writing - review & editing. **M. Pasturel:** Supervision, Writing - review & editing. **H. Palancher:** Project administration, Supervision, Writing - review & editing.

Declaration of interests

The authors declare that they have no known competing financial interests or personal relationships that could have appeared to influence the work reported in this paper.

The authors declare the following financial interests/personal relationships which may be considered as potential competing interests:

REFERENCES

- [1]. M. Durazzo, E. Vieira, E.F. Urano de Carvalho, H.G. Riella, *Evolution of fuel plate parameters during deformation in rolling*, Journal of Nuclear Materials 490 (2017) 197-210. <https://doi.org/10.1016/j.jnucmat.2017.04.018>
- [2]. A. Travelli, *Current status of the RERTR program*, RERTR international meeting, Argonne, USA, 1980.
- [3]. J.L. Snelgrove, G.L Hofman, C.L. Trybus, T.C. Wiencek, *Development of very-high-density fuels by the RERTR program*, RERTR international meeting, Seoul, Republic of Korea, 1996.
- [4]. C.K. Kim, J.M. Park, H.J. Ryu, *Use of centrifugal atomization process in the development of research reactor fuel*, Nuclear Engineering and Technology 39 (2007) 617-626. <https://doi.org/10.5516/NET.2007.39.5.617>
- [5]. A. Leenaers, J. Wight, S. Van den Berghe, H.J. Ryu, J.F. Valery, *U-Mo based fuel system*, Comprehensive Nuclear Materials (2nd Edition) section 5.16 (2020) 499-530.
- [6]. A. Leenaers, J. Wight, S. Van den Berghe, H.J. Ryu, J.F. Valery, *U-Si based fuel system*, Comprehensive Nuclear Materials (2nd Edition) section 5.15 (2020) 485-498.
- [7]. J.M. Harp, P.A. Lessing, R.E. Hoggan, *Uranium silicide pellet fabrication by powder metallurgy for accident tolerant fuel evaluation and irradiation*, Journal of Nuclear Materials 466 (2015) 728-738. <https://doi.org/10.1016/j.jnucmat.2015.06.027>
- [8]. J. Havette, X. Iltis, H. Palancher, D. Drouan, O. Fiquet, E. Castelier, M. Pasturel, *From arc-melted ingot to MTR fuel plate: A SEM/EBSD microstructural study of U₃Si₂*, Journal of Nuclear Materials 537 (2020) 152224. <http://doi.org/10.1016/j.jnucmat.2020.152224>

- [9]. J.P. Durand, B. Duban, Y. Lavastre, S. de Perthuis, *CERCA's 25 years experience in U₃Si₂ fuel manufacturing*, RERTR international meeting, Chicago, USA, 2003.
- [10]. X.S. Wang, Y. Xu, *Mechanical characterizations of the dispersion U₃Si₂-Al fuel plate with sandwich structure*, Applied Composite Materials 10 (2003) 159-167. <https://doi.org/10.1023/A:1023978413329>
- [11]. C.K. Kim, K.H. Kim, D.B. Lee, *High U-density nuclear fuel development with application of centrifugal atomization technology*, Seminar on the new fuel technology towards the 21th century, Taejon, Republic of Korea, 1997.
- [12]. K.H. Kim, D.B. Lee, C.K. Kim, I.H. Kuk, K.W. Paik, *Characteristics of U₃Si and U₃Si₂ powders prepared by centrifugal atomization*, Journal of Nuclear Science and Technology 34 (1997) 1127-1132. <https://doi.org/10.1080/18811248.1997.9733801>
- [13]. K.H. Kim, J.M. Park, C.K. Kim, G.L. Hofman, K.W. Paik, *Thermal compatibility studies of U₃Si₂ dispersion fuels prepared with centrifugally atomized powder*, Journal of Nuclear Materials 270 (1999) 315-321. [https://doi.org/10.1016/S0022-3115\(99\)00005-7](https://doi.org/10.1016/S0022-3115(99)00005-7)
- [14]. J.M. Park, Y.J. Jeong, K.H. Lee, K.N. Kim, S.H. Kim, T.W. Cho, J.S. Yim, Y.W. Tahk, H.J. Kim, *Evolution of KAERI fuel fabrication capability*, RERTR international meeting, on-line, 2021.
- [15]. J.H. Yang, D.S. Kim, D.J. Kim, S. Kim, J.H. Yoon, H.S. Lee, Y.H. Koo, K.W. Song, *Oxidation and phase separation of U₃Si₂ nuclear fuel in high-temperature steam environment*, Journal of Nuclear Materials 542 (2020) 152517. <https://doi.org/10.1016/J.JNUCMAT.2020.152517>
- [16]. *Safety evaluation report related to the evaluation of low-enriched silicide-aluminum dispersion fuel for use in non-power reactors*, NUREG-1313 report, U.S. Nuclear Regulatory Commission, 1988.
- [17]. Y.J. Jeong, S.H. Kim, H.Y. Song, D.H. Kang, C.H. Park, K.H. Lee, K.N. Kim, J.M. Park, *Current status on the development of high-density LEU U₃Si₂ fuel in KAERI*, RERTR international meeting, Zagreb, Croatia, 2019.
- [18]. X. Iltis, I. Zacharie-Aubrun, H.J. Ryu, J.M. Park, A. Leenaers, A.M. Yacout, D.D. Keiser, F. Vanni, B. Stepnik, T. Blay, N. Tarisien, C. Tanguy, H. Palancher, *Microstructure of as-atomized and annealed U-Mo7 particles: A SEM/EBSD study of grain growth*, Journal of Nuclear Materials 495 (2017) 249-266. <https://doi.org/10.1016/j.jnucmat.2017.07.056>
- [19]. J. Rodriguez-Carjaval, *Recent advances in magnetic structure determination by neutron powder diffraction*, Physica B 192 (1993) 55-69. [https://doi.org/10.1016/0921-4526\(93\)90108-I](https://doi.org/10.1016/0921-4526(93)90108-I)
- [20]. A. Giannuzzi, F.A. Stevie, *Introduction to focused ion beams: instrumentation, theory, techniques and practice*, Springer, 2005.
- [21]. M. Klinger, *CrysTBox – Crystallographic Toolbox*, Institute of Physics of the Czech Academy of Science (2015).
- [22]. D. Chen, J.C. Kuo, W.T. Wu, *Effect of microscopic parameters on EBSD spatial resolution*, Ultramicroscopy 111 (2011) 1488-1494. <https://doi.org/10.1016/j.ultramic.2011.06.007>
- [23]. W.H. Zachariasen, *Crystal Chemical Studies of the 5f-Series of Elements. VIII. Crystal structure studies of uranium silicides and of CeSi₂, NpSi₂, and PuSi₂*, Acta Crystallographica 2 (1949) 94–99. <https://doi.org/10.1107/S0365110X49000217>

- [24]. R. Pöttgen, D. Kaczorowski, W. Jeitschko, *Crystal structure, magnetic susceptibility and electrical conductivity of the uranium silicide carbides $U_3Si_2C_2$ and $U_{20}Si_{16}C_3$* , Journal of Materials Chemistry 3 (1993) 253–258. <https://doi.org/10.1039/JM9930300253>
- [25]. P. Rogl, H. Noël, *The C-Si-U system (Carbon-Silicon-Uranium)*, Journal of Phase Equilibria 16 (1995) 66-72. <https://doi.org/10.1007/BF02646251>
- [26]. H. Noël, V. Queneau, J.P. Durand, P. Colomb, *Characterization of a new binary uranium silicide*, Abstracts of the Conference on strongly correlated systems (SCES98), Paris, France, 1998.
- [27]. D.A. Lopes, V. Kocevski, T.L. Wilson, E.E. Moore, T.M. Besmann, *Stability of U_5Si_4 phase in U-Si system: crystal structure prediction and phonon properties using first-principles calculations*, Journal of Nuclear Materials 510 (2018) 331-336. <https://doi.org/10.1016/j.jnucmat.2018.08.026>
- [28]. T.L. Ulrich, S.C. Vogel, D.A. Lopez, V. Kocevski, J.T. White, E.S. Sooby, T.M. Besmann, *Phase stability of U_5Si_4 , USi , and U_2Si_3 in the uranium-silicon system*, Journal of Nuclear Materials 540 (2020) 152353. <https://doi.org/10.1016/j.jnucmat.2020.152353>
- [29]. C.T. Kniess, E.F.U. Carvalho, M. Durazzo, H.G. Riella, *Quantitative determination of crystalline phases in the silicide fuel by the Rietveld method*, RRFM 2010, March 21-25, Marrakech, Morocco.
- [30]. R.H.L. Garcia, A.M. Saliba-Silva, E.F.U. Carvalho, N.B. Lima, R.U. Ichikawa, L.G. Martinez, *Characterization of uranium silicide powder using XRD*, International Nuclear Atlantic Conference (INAC), Recife, Brazil, 2013.
- [31]. W. Pitschke, N. Mattern, H. Hermann, *Incorporation of microabsorption corrections into Rietveld analysis*, Powder Diffraction 8 (1993) 223-228. <https://doi.org/10.1017/S0885715600019412>
- [32]. S.C. Middleburgh, R.W. Grimes, E.J. Lahoda, C.R. Stanek, D.A. Andersson, *Non-stoichiometry in U_3Si_2* , Journal of Nuclear Materials 482 (2016) 300-305. <https://doi.org/10.1016/j.jnucmat.2016.10.016>
- [33]. K. Persson, *Materials Data on $U_{20}Si_{16}C_3$ (SG:191) by Materials Project*, Materials Project Database. <https://doi.org/10.17188/1197244>
- [34]. D. Berthebaud, O. Tougait, A.P. Gonçalves, H. Noël, *Phase relations and stabilities at 900°C in the U-Fe-Si ternary system*, Intermetallics 16 (2008) 373-377. <https://doi.org/10.1016/j.intermet.2007.11.007>
- [35]. H. Noël, P.F. Rogl, *The ternary system: silicon-uranium-vanadium*, Journal of Nuclear Materials 404 (2010) 77-81. <https://doi.org/10.1016/j.jnucmat.2010.06.033>
- [36]. G. Leinders, T. Cardinaels, K. Binnemans, M. Verwerft, *Low-temperature oxidation of fine UO_2 powders: thermochemistry and kinetics*, Inorganic Chemistry 57 (2018) 4196-4204. <https://doi.org/10.1021/acs.inorgchem.6b00127>
- [37]. T.B. Massalski, H. Okamoto, P.R. Subramanian, L. Kacprzak, *Binary alloy phase diagrams (2nd edition)*, ASM International (1990).
- [38]. A. Berche, R. Rado, O. Rapaud, C. Guéneau, J. Rogez, *Thermodynamic study of the U-Si system*, Journal of the Nuclear Materials 389 (2009) 101-107. <https://doi.org/10.1016/j.jnucmat.2009.01.014>
- [39]. R.E. Hoggan, K.R. Tolman, F. Cappia, A.R. Wagner, J.M. Harp, *Grain size and phase purity characterization of U_3Si_2 fuel pellets*, Journal of Nuclear Materials 512 (2018) 199-213. <https://doi.org/10.1016/j.jnucmat.2018.10.011>

- [40]. N. Ciftci, N. Ellendt, G. Coulthard, E. Soares Barreto, L. Mädler, V. Uhlenwinkel, *Novel cooling rate correlations in molten metal gas atomization*, Metallurgical and Materials Transactions B 50 (2019) 666-677. <https://doi.org/10.1007/s11663-019-01508-0>
- [41]. T. Nagaze, K. Mizuuchi, T. Nakano, *Solidification microstructure of the ingots obtained by arc melting and cold crucible levitation melting in TiNbTaZr medium-entropy alloy and TiNbTaZrX (X= V, Mo, W) high entropy alloys*, Entropy 21 (2019) 483. <https://doi.org/10.3390/e21050483>
- [42]. A. Bonnin, J.P. Wright, R. Tucoulou, H. Palancher, *Impurity precipitation in atomized particles evidenced by nano X-ray diffraction computed tomography*, Applied Physics Letters 105 (2014) 084103. <https://doi.org/10.1063/1.4894009>
- [43]. E. Gil, J. Cortés, I. Iturriza, N. Ordás, *XPS and SEM analysis of gas atomized powder precursor of ODS ferritic steels obtained through the STARS route*, Applied Surface Science 427 (2018) 182-191. <https://doi.org/10.1016/j.apsusc.2017.07.205>
- [44]. D. Riabov, E. Hryha, M. Rashidi, S. Bengtsson, L. Nyborg, *Effect of atomization on surface oxide composition in 316L stainless steel powders for additive manufacturing*, Surface and Interface Analysis 52 (2020) 694-706. <https://doi.org/10.1002/sia.6846>
- [45]. A.A. Solomon, S. Revankar, J.K. McCoy, *Thermal conductivity oxide fuels*, Final report n° 02-180, Award N° DE-FG07-02SF22613, 2006.
- [46]. T. Zweifel, Ch. Valot, Y. Pontillon, J. Lamontagne, A. Vermersch, L. Barrallier, T. Blay, W. Petry, H. Palancher, *Annealing tests of in-pile irradiated oxide coated U-Mo/Al-Si dispersed nuclear fuel*, Journal of Nuclear Materials 452 (2014) 533-547. <https://doi.org/10.1016/j.jnucmat.2014.05.052>
- [47]. R.C. Birtcher, J.W. Richardson, M.H. Mueller, *Amorphization of U_3Si_2 by ion and neutron irradiation*, Journal of Nuclear Materials 230 (1996) 158-163. [https://doi.org/10.1016/0022-3115\(96\)00160-2](https://doi.org/10.1016/0022-3115(96)00160-2)
- [48]. T. Yao, B. Gong, L. He, Y. Miao, J.M. Harp, M. Tonks, J. Lian, *In-situ TEM study of the ion irradiation behavior of U_3Si_2 and U_3Si_5* , Journal of Nuclear Materials 511 (2018) 56-63. <https://doi.org/10.1016/j.jnucmat.2018.08.058>